

論文 / 著書情報
Article / Book Information

題目(和文)	
Title(English)	Study of Surface Wave Mechanisms Applicable to Thrusters for Watertight Mobile Robots
著者(和文)	傅幼均
Author(English)	Yu-Chun Fu
出典(和文)	学位:博士(工学), 学位授与機関:東京工業大学, 報告番号:甲第9453号, 授与年月日:2014年3月26日, 学位の種別:課程博士, 審査員:福島 E 文彦,大熊 政明,小田 光茂,松永 三郎,中島 求,塚 越 秀行,廣瀬 茂男
Citation(English)	Degree:Doctor (Engineering), Conferring organization: Tokyo Institute of Technology, Report number:甲第9453号, Conferred date:2014/3/26, Degree Type:Course doctor, Examiner:,,,,,,
学位種別(和文)	博士論文
Type(English)	Doctoral Thesis

Study of Surface Wave Mechanisms
Applicable to Thrusters for Watertight Mobile Robots

Yu-Chun Fu

Department of Mechanical and Aerospace Engineering
Tokyo Institute of Technology

February 2014

A thesis presented

by

Yu-Chun FU

to

The Department of Mechanical and Aerospace Engineering

in partial fulfillment of the requirements

for the degree of

Doctor of Engineering

Academic Advisors:

Professor Shigeo Hirose

Assoc. Professor Edwardo F. Fukushima

Tokyo Institute of Technology

Tokyo, Japan

February, 2014

Abstract

This research aims to develop a new propulsion mechanism, “Surface Wave Mechanism,” which generates propulsive force by wavy motion. It features in large propulsion area, no exposed infinite rotating shaft, and water and dust proof structure. First, this study investigated present mobile robots relating to surface wave. Then, three types of Surface Wave Mechanism were proposed. After the basic motion experiments of each prototype, this research focused on the development of Rotary Surface Wave (RS-Wave) Mechanism, which has a novel and unique design. The basic concept, analysis of design parameters, and the experimental results of the prototype are presented in this thesis. In addition, a mobile vehicle applied RS-Wave mechanism was made and evaluated experimentally. The propulsion ability of RS-Wave mechanism was confirmed and it would probably find application in inspection robots. Furthermore, for improving the locomotion efficiency, a load-sensitive mechanism for RS-Wave mechanism was also proposed. Feasibility of load-sensitive RS-Wave mechanism was confirmed experimentally.

Acknowledgement

I would like to express my sincere gratitude to my advisor, Professor Shigeo Hirose, who has been a tremendous mentor for me. He kindly provided me the chance to enter this lab and study under his guidance, and kept supporting me even after his retirement. His passion and creativity in robotics have inspired me a lot. Without his support and guidance, I would not be able to accomplish this research.

I would like to thank Associate Professor Edwardo F. Fukushima, who also provided me lots of guidance and assistance especially in the last year. I also want to thank Assistant Professor Gen Endo, who provided me with his experience and advice.

I would also like to thank every lab members who helped me with my research, and offered a harmonious and warm atmosphere in the lab. Especially thanks to Dr. Koji Ueda, who gave me a lot of support and assistance in the experiments. Also thanks to Dr. Hiroya Yamada, Mr. Satoshi Kitano, Mr. Yuki Murayama, and Mr. Jose Antonio Silva for providing advice and assisting with my experiments. Thanks to Mr. Ben Allan for correcting my English writing.

I also want to show my deep appreciation to Tokyu Foundation for Foreign Students who provide me with scholarship so that I could be concentrate on the study without worrying about living expenses. More importantly, the warm and happy events in Tokyu Foundation supported me a lot spiritually.

Finally, I must show my deepest gratitude to my family. Even though I am

living far away from them, I can feel their love and support all the time. It is their encouragement and support that helps me to finish my research successfully.

Contents

Abstract	ii
Acknowledgement	iv
1 Introduction	1
1.1 Background	1
1.2 Requirement of Mobile Robot	2
1.3 Difficulties on Present Propulsion Mechanism	3
1.4 Proposal of Surface Wave Mechanism	4
1.5 Structure of this Thesis	5
1.6 Chapter Summary	7
2 Related Former Studies	9
2.1 Former Studies	9
2.2 Classification of Surface Wave Mechanism	12
2.2.1 Type of the wave	12
2.2.2 Allocation of driving system	13
2.3 Purpose of this Research	15
2.4 Chapter Summary	15
3 Development of Perpendicular Type Surface Wave Mechanism	17
3.1 Surface Wave Mechanism PD-I	17

3.1.1	Concept	17
3.1.2	Mechanical Design	18
3.1.3	Experiment and Result	19
3.1.4	Review and Modification	21
3.1.5	Experimental Result of the Modified Model	24
3.1.6	Discussion	25
3.2	Surface Wave Mechanism PD-II	26
3.2.1	Concept	26
3.2.2	Mechanical Design	27
3.2.3	Watertight Design	28
3.2.4	Motion Experiment	29
3.2.5	Underwater Experiment	32
3.2.6	Discussion	34
3.3	Chapter Summary	35
4	Development of Parallel Type Surface Wave Mechanism	37
4.1	Concept	37
4.2	Motion Analysis and Simulation	39
4.3	The First Prototype	47
4.3.1	Mechanical Design	47
4.3.2	Experiment and Result	49
4.3.3	Modification and Torque Measurement	50
4.4	Chapter Summary	52
5	Development of RS-Wave Vehicle	53
5.1	Modification of RS-Wave Mechanism	53
5.2	Mechanical Design	57
5.3	Motion Control	58

5.4	Experiment and Result	59
5.4.1	Underwater	60
5.4.2	Narrow Space	61
5.4.3	Slope	64
5.4.4	Step	64
5.4.5	Soft Ground	65
5.4.6	Flipped Over	66
5.4.7	Summary of Experimental Result	67
5.5	Energy Efficiency of RS-Wave Vehicle	67
5.5.1	Introduction of Specific Resistance	67
5.5.2	Experiment on RS-Wave Vehicle	68
5.5.3	Energy Loss of Bellows	71
5.6	Chapter Summary	72
6	Load-sensitive RS-Wave Mechanism	73
6.1	Introduction of Load-sensitive Mechanism	73
6.2	RS-Wave Mechanism With Load-sensitive Mechanism	74
6.3	Mechanical Design	77
6.4	Experiment and Result	83
6.4.1	Propulsive motion with fixed inclination	83
6.4.2	Effect of load-sensitive mechanism	86
6.5	Discussion	89
6.6	Chapter Summary	90
7	Conclusions and Future Work	91
7.1	Conclusion	91
7.2	Possible Applications of RS-Wave Mechanism	93

7.2.1	Inspection Robot	93
7.2.2	In-pipe Robot	94
7.3	Future Work	94
7.4	Chapter Summary	96
	Bibliography	97
	Appendix A CAD Drawings	103
	Appendix B Trajectory Simulation	107
	Appendix C Calculation of Contact Angle α	111

List of Figures

1.4.1 Concept of Surface Wave Mechanism	4
1.5.1 Structure of this thesis	7
2.1.1 Earthworm-like robot	10
2.1.2 Toroidal robot	10
2.1.3 Screw driven vehicle (Neumeyer and Jones,1965)	11
2.1.4 Centipede robot (Koh et al.,2010)	12
2.2.1 Allocation of rotating shaft	13
3.1.1 Design concept of PD-I	18
3.1.2 Rotating motion caused by eccentric cylinder	18
3.1.3 Structure of PD-I	19
3.1.4 Motion experiment of PD-I	20
3.1.5 Inclinations of rubber pads cause unsteadiness	21
3.1.6 Modification of contact part	22
3.1.7 Structure of modified PD-I	23
3.1.8 Structure of the legs of modified PD-I	23
3.1.9 Motion Experiment of modified PD-I	24
3.1.10Modification of contact point	25
3.2.1 Crankshaft	26
3.2.2 Structure of PD-II	27

3.2.3 Crankshaft of PD-II	28
3.2.4 Bottom view of PD-II	28
3.2.5 Watertight design of PD-II	29
3.2.6 Motion experiment	30
3.2.7 Proceeding speed of PD-II	31
3.2.8 Slope climbing experiment	32
3.2.9 Watertightness experiment	33
3.2.10 Top view of underwater experiment	33
3.2.11 Side view of underwater experiment	34
3.2.12 Image of triangle structure	35
4.1.1 Eccentric inclined plate	38
4.1.2 Rotating motion generated by the rim of eccentric inclined disc	38
4.2.1 Circle C_1 on xy -plane	40
4.2.2 Inclined circle C_2	41
4.2.3 Eccentric inclined circle C_3	41
4.2.4 Rotate \mathbf{P}_3 along z -axis	42
4.2.5 Simulation result of Rotary Surface Wave Mechanism	44
4.2.6 Shape of the trajectory in different views	44
4.2.7 Trajectory of different inclination	45
4.2.8 Trajectory of different eccentricity	45
4.2.9 Size of trajectory	46
4.3.1 Prototype of RS-Wave Mechanism	48
4.3.2 Eccentric inclined plate unit	48
4.3.3 Overview of RS-Wave Mechanism	49
4.3.4 Motion experiment	50
4.3.5 Adjustable parts	51

4.3.6 Torque under different inclinations and eccentric distances	52
5.1.1 Structure of RS-Wave unit	54
5.1.2 Planetary gear set	54
5.1.3 Design of the eccentric inclined disc unit	54
5.1.4 Trajectory of propulsive motion	56
5.1.5 Patterns of RS-Wave units connection	57
5.2.1 Appearance of RS-Wave vehicle	58
5.3.1 Control circuit of RS-Wave Vehicle	59
5.3.2 Control box of RS-Wave Vehicle	59
5.4.1 Pivot turning of RS-Wave vehicle	60
5.4.2 Underwater experiment	61
5.4.3 Narrow space	62
5.4.4 Propulsion under 31.5kg load	63
5.4.5 Speed and current under load	63
5.4.6 Slope climbing experiment	64
5.4.7 Step climbing experiment	65
5.4.8 Motion on soft ground	66
5.4.9 Interference of returning phase	66
5.5.1 Three types of power measurement	69
5.5.2 Specific resistance ε calculated with P_L	70
5.5.3 Specific resistance ε calculated with P_{net}	70
5.5.4 Specific resistance of other vehicles	71
5.5.5 RS-Wave vehicle without bellows	72
6.2.1 Thrusting force of RS-Wave mechanism (Top view)	75
6.2.2 Tangent angle at contact point	76
6.2.3 Concept of load-sensitive RS-Wave mechanism	77

6.3.1 Experiment device for load-sensitive RS-Wave mechanism	78
6.3.2 Experiment installation	79
6.3.3 Disc for load-sensitive experiment	80
6.3.4 Disc fixed on the rotating shaft	81
6.3.5 Effect of the eccentricity direction to ground-contacting region	82
6.3.6 Electrical system of experiment device	82
6.4.1 Propelling displacement under varying payload	85
6.4.2 Variation of inclination and propelling displacement	88
6.4.3 Variation of contact angle and propelling displacement	88
6.5.1 Contacting region of the disc	90
7.2.1 Underfloor inspection robot	93
7.2.2 In-pipe robot using RS-Wave mechanism	94
7.3.1 Synchronized load-sensitive RS-Wave mechanism	95
A.0.1 Drawing of Surface Wave Mechanism PD-I	104
A.0.2 Drawing of Surface Wave Mechanism PD-II	105
A.0.3 Drawing of Surface Wave Mechanism PL-I	106

List of Tables

2.2.1 Classifications of related propulsion mechanisms	14
3.1.1 Specifications of PD-I	19
3.1.2 Specifications of modified PD-I	23
3.2.1 Specifications of PD-II	28
4.3.1 Specifications of the Prototype	49
5.1.1 Dimensions of eccentric inclined disc unit	55
5.2.1 Specifications of the RS-Wave Vehicle	58
6.3.1 Specification of electronic devices	83
6.4.1 Experiment condition	86
7.1.1 Comparison of the three proposed Surface Wave Mechanisms	92

Chapter 1

Introduction

1.1 Background

Urban infrastructure decay has become an important issue for developed and developing countries in recent years. In the case of Japan, the World War II destroyed most of the industrial plants and infrastructures, thus a lot of infrastructures and buildings were built in the postwar years. Several decades have past, those infrastructures and buildings are now decaying and need maintaining or renewing. According to the Cabinet Office of Japan, the transportation infrastructure which have been used for over 50 years will exceed fifty percent of the total amount [1]. Since Japan is located in an earthquake zone and earthquakes occur frequently, it is important and urgent to inspect all the structures which have potential risk.

Regarding to the infrastructures such as tunnels, sewers, underground pipelines, or floors and ceilings of buildings, it is difficult and sometimes even dangerous for people to do the inspection tasks inside. There are several reasons; firstly, the inspecting object may be frail and there is a possibility that it collapses in any moment. Besides, some of the inspecting objects involve really narrow space where human beings cannot reach. Moreover, the environment tends to be dark and dirty and full

of dust, which is not only uncomfortable but also harmful for health. Therefore, a mobile robot that can accomplish the inspection works instead of human is in demand. The development of inspection robots has been a popular research subject in robotics field.

1.2 Requirement of Mobile Robot

Regarding to the conditions of operating environment for inspection robot, an ideal inspection robot must meet several requirements. Some important requirements are listed and explained in the followings.

- **Simple and robust design**

Since the mobile robots are expected to operate in difficult environment that usually include lots of rough terrains, it is better to have a simple and robust design so that they will not break easily. Besides, if the structure of the mobile robot is too complex, the cost also increases and it is not practical for applications.

- **Waterproof and dust-proof design**

The condition of inspection fields are unpredictable. For example, underfloor area may be full of dust, scattered wires, or even leak of water. Besides, an inspecting operation outdoor has the chance to encounter sudden rain. Therefore, the inspection robot must be waterproof and dust-proof.

- **Large output force**

In case the robots need to squeeze through narrow interval, or be pressed by any fallen obstacle, they may need to operate under large load, otherwise it is

easily to get stuck. Hence, the mobile robot must bear heavy load and output large thrusting force.

- **Terrain adaptation**

To be able to accomplish inspection operations, the mobile robot must have high mobility and be able to overcome different terrain conditions. For example, there might be some pipelines or pillars that standing or lying on the ground in underfloor area, the mobile robots needs to be able to cross over these obstacles by itself.

- **Slim body**

Since the inspection mobile robots are expected to operate in narrow space, it is better to have a slim body so that the robot can move in narrow space easily.

1.3 Difficulties on Present Propulsion Mechanism

The most commonly used propulsion mechanism for mobile robots are wheels, crawlers, and legs. In particular, Wheels and crawlers are widely used for rescue robots [2]. They have good efficiency and stability in locomotion. However, wheels and crawlers have some defects; such as getting stuck when the mobile robot is overturned or when some strings tangle with their infinite rotating shafts. Leg robots are good at locomotion on rough terrain, but they usually require lots of actuators and complex control system.

Besides those common propulsion mechanism mentioned above, several mobile robots with different propulsion mechanisms have been studied. For example, an active flexible cable that is driven by ciliary vibration mechanism [3, 4]. It had

a simple structure, but the mobility of this kind of propulsion mechanism is not efficient. Another example is Slim Slime Robot[5], which is capable of generating various types of locomotion. However, the structure was rather complex.

1.4 Proposal of Surface Wave Mechanism

The objective of this research is to develop a new propulsion mechanism which has high mobility, a simple structure, and can be easily sealed against water and dust. Considering these targets, a new mechanism called “Surface Wave Mechanism” was proposed. The basic concept of Surface Wave Mechanism is generating wave motion on the surface of the body, and then use the wave motion to produce propulsion for the vehicle. The concept of Surface Wave Mechanism is sketched in Fig. 1.4.1. There is a series of small scale rotation device in a row, and each rotation device has some phase differences between each other. The blue points on the surface move in circular reciprocate motion. In every rotation cycle, the blue points generate propulsion while contact to the ground and then lifts up in the rest period of the cycle. As a result, the whole mechanism moves forward.

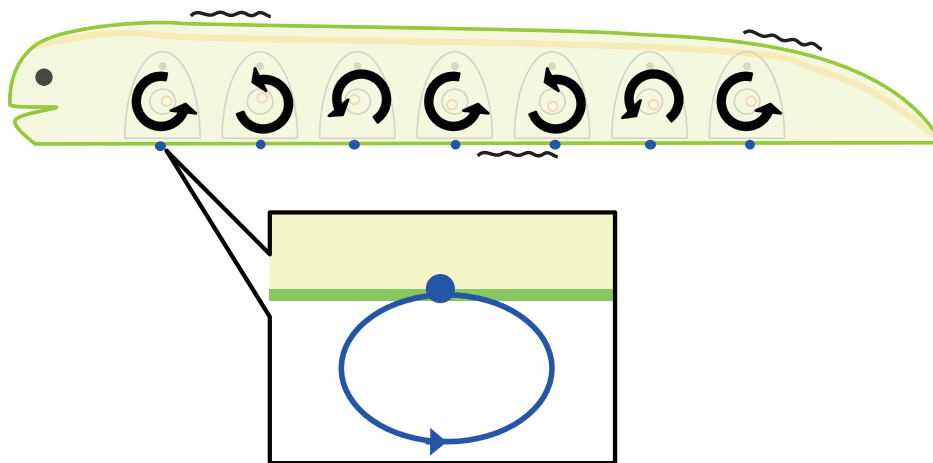


Fig. 1.4.1: Concept of Surface Wave Mechanism

There are mainly two advantages of propelling by Surface Wave Mechanism.

1. **Large propulsive surface**

By generating wave motion from the whole body surface, the mechanism has a large area that is generating propulsive force. This feature improves mobility of robots that operate in rough terrain.

2. **No exposed infinite rotating shaft**

An exposed infinite rotating shaft may get tangled with wires or strings and then stuck. But a Surface Wave Mechanism dose not have this risk. Moreover, it can be sealed against water and dust easily by wrapping up with watertight cover.

With these advantages, Surface Wave Mechanism is considered to be suitable for inspection mobile robots in severe environment. In particular, for the environment which has narrow space and be covered with dust, Surface Wave Mechanism might be preferred.

This study aims in development of Surface Wave Mechanism. Several different designs had been proposed, and the prototypes had been made and evaluated. The following chapters will present the development process in detail, including the basic concept, the mechanical design, and the experimental results of the developed prototypes of Surface Wave Mechanism.

1.5 Structure of this Thesis

This thesis is composed of seven chapters. Fig. 1.5.1 shows the structure of the thesis.

Chapter 1 Introduction, this chapter, gives an overview of the research background and introduced the concept of Surface Wave Mechanism.

Chapter 2 Related Former Studies introduces and categorizes present propulsion mechanisms that are related to Surface Wave Mechanism. In this study, the existing related mechanisms are categorized by two methods. One is according to the type of wave, either travelling wave or stationary wave. The other is according to the allocation of driving shaft and proceeding orientation, either perpendicular type or parallel type. The characteristics of each type are discussed.

Chapter 3 Development of Perpendicular Type Surface Wave Mechanism presents the development of Surface Wave Mechanism PD-I and PD-II. PD-I generated propulsion by vibration, and PD-II utilized crankshaft for steady propulsion. The prototypes design and experimental results are explained.

Chapter 4 Development of Parallel Type Surface Wave Mechanism presents the development of Surface Wave Mechanism PL-I, which is also named Rotary Surface Wave (RS-Wave) mechanism. It possesses a novel structure which generate propulsion on the whole cylindrical body by using only a single actuator. The concept, mechanical design, and experiment result are presented. Besides, some important design parameters of RS-Wave mechanism are discussed.

Chapter 5 Development of RS-Wave vehicle introduces the first application of RS-Wave mechanism on a vehicle. First, the modified RS-Wave mechanism with a more compact design is presented. Then, a vehicle that composed of two RS-Wave units is designed. The performance of the vehicle are evaluated in the chapter.

Chapter 6 Load-sensitive RS-Wave Mechanism proposes a load-sensitive mechanism to improve the efficiency of RS-Wave mechanism. With load-sensitive mechanism, the propulsion mechanism may adjust its output thrusting force and velocity according to the environment condition. The design of experiment device and the experiment result are explained.

Chapter 7 Conclusions and Future Work gives final comments and con-

clusions to summarize the contents of this thesis and suggests methods for further modification or application of RS-Wave mechanism. Some possible application examples of RS-Wave mechanism are discussed.

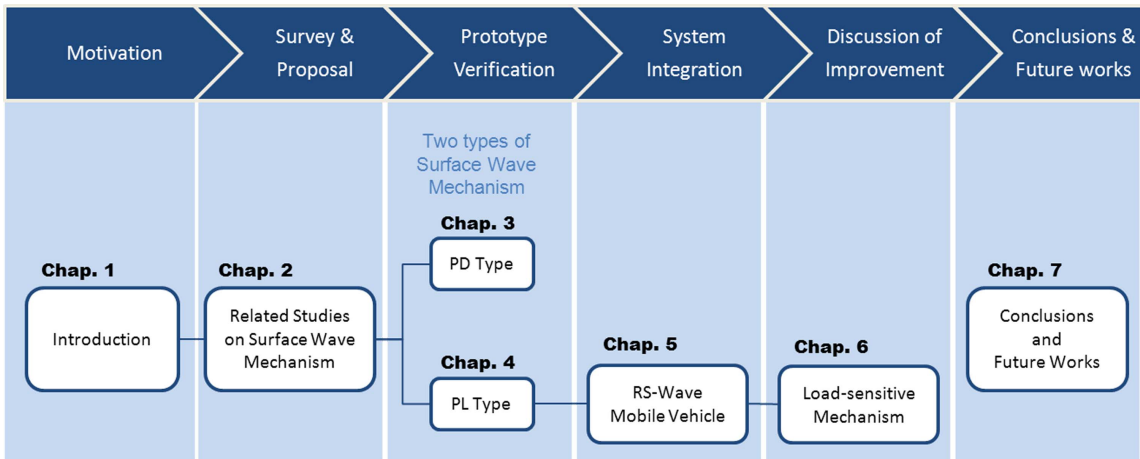


Fig. 1.5.1: Structure of this thesis

1.6 Chapter Summary

This chapter presented the overview of this research. First, the needs of inspection mobile robot were explained. Then, the basic requirements of those mobile robot were listed. Finally, a new concept of propulsion mechanism named “Surface Wave Mechanism” was proposed.

Chapter 2

Related Former Studies

2.1 Former Studies

In this chapter, we would like to present a general view of related former studies. Although the term “Surface Wave Mechanism” had not been proposed in the field of mobile robot before, there are several existing robots that use similar concept for locomotion. These mechanisms have either propelling skin or wavy motion. Some related mechanisms are listed below:

- **Earthworm/inchworm-like robot**

Many robots use peristaltic motion for locomotion, which is inspired by the motion of earthworm or inchworm. This type of robot basically generates forward motion by the contraction and expansion of the body segments, and it is widely used on in-pipe robot [6–8]. There are various actuating system for generating peristaltic motion; Many of them were driven by pneumatic or hydraulic actuators [5, 7–9]; while Omori et al. used servo motors and crank mechanism [6]; and Kim et al. applied shape memory alloy [10].



(a) Omori et al.,2008



(b) Boxerbaum et al.,2010

Fig. 2.1.1: Earthworm-like robot

- **Toroidal mechanism**

The skin of the robot forms a loop, and by continuously reversing the loop, the robot can move forward. This concept has been applied to many robots [11–15]. The entire external surface of the robot provides continuous propulsive force, thus the locomotion is fast and steady. However, since the skin of the robot is continuously reversing, the sealing against dust and water is difficult. Kimura et al. made the robot which was hermetically sealed, but the size of the robot was rather big.



(a) McKenna et al.,2008



(b) Kimura et al.,2006

Fig. 2.1.2: Toroidal robot

- **Screw driven vehicle**

This type of vehicle use screw-type device for propulsion. There has been a long history of the screw driven vehicle. Colonel John Stevens built the first practical screw-driven steamboat in 1804 [16]. Later on, several screw-driven amphibious vehicles had been developed [17, 18]. This kind of vehicle is good at locomotion on soft ground, such as snow, mud or swamp, but it is not good for locomotion on normal dry land [19]. Thrusting motion of the screw driven mechanisms is based on the sliding on the surface of the screw, so energy efficiency is not good. Besides off-road vehicles, screw drive-type device was also applied to in-pipe capsule robot [20].

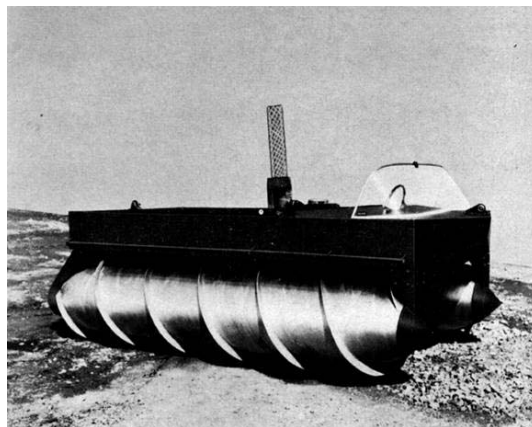


Fig. 2.1.3: Screw driven vehicle (Neumeyer and Jones,1965)

- **Multi-leg robot**

Some multi-leg robots use their leg to generate ripple gait motion. The centipede robot in Fig. 2.1.4 is an example [21]. Another example is a snake-like robot [22] which also propelled by its feet on multi-segment body. Similar motion can also be found in some animated toys [23–26], the legs were connected by linkages such as gears or crankshafts. When the linkages were driven, they could generate synchronized propelling motions. These robots had good mo-

bility, but the rotating legs of course have exposed infinite rotating shaft and difficult to make it water and dust tight.



Fig. 2.1.4: Centipede robot (Koh et al.,2010)

2.2 Classification of Surface Wave Mechanism

In this study, the present existing mechanisms that related to surface wave mechanism were categorized based on two characteristics. One is the type of the propulsive wave generated, the other is the allocation of the driving system.

2.2.1 Type of the wave

With regard to wave motions of this type of mechanisms, they can be categorized to two types:

1. **Travelling wave:** All the particles on the wave is moving toward one direction.

The toroidal mechanisms are classified to this type. Another example is screw drive mechanism, the particles in between the treads move forward while the screw rotates. Travelling wave may be efficient in propulsion since the whole surface is moving to the same direction.

2. **Stationary wave:** The wave that always remains in a constant position, and the particles on the wave only make reciprocating motion.

The earthworm/inchworm-like robots and multi-leg robots are categorized to this type. Another example is the rescue robot Bari-Bari-II [27] which is propelled by a two-mode alternating step structure. The spiral style wave transmission system[28] is a special example. It had similar structure as screw drive mechanism, but the screws were covered by sponge rubber which transmitted the wave. It can be categorized as a stationary wave mechanism. Stationary wave mechanism is easier to seal by covering watertight coating since the particles on the wave only move in certain small region.

2.2.2 Allocation of driving system

As for the actuating systems, some mechanisms are electric actuated and some are hydraulic or pneumatic actuated. For those electric actuated mechanisms, they can be further classified into two different types as shown in Fig. 2.2.1.

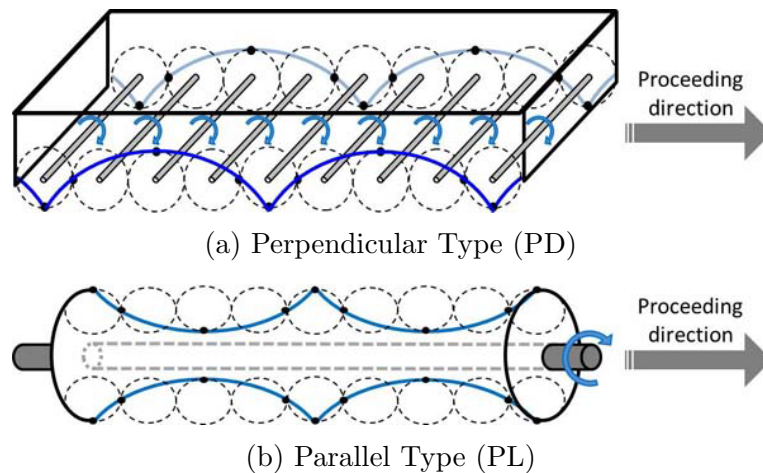


Fig. 2.2.1: Allocation of rotating shaft

1. **Perpendicular type** (hereinafter referred to as “PD”): The axis of rotating shaft is perpendicular to its proceeding direction.

This type is more common on the existing mechanisms, for example wheel or crawler vehicles. In the above mentioned mechanisms, those multi-leg robots and some of the toroidal mechanism actuated by motors can be categorized to this type.

2. **Parallel type** (hereinafter referred to as “**PL**”): The axis of rotating shaft is parallel to the proceeding direction.

The screw driven vehicle is a distinct example of this category. Besides that, a pipe-line robot Thes-I [29] also belong to this type. As PL type mechanism can generate wavy motion by the central shaft, it is considered to be more compact for mobile robot that enters narrow space.

Table 2.2.1: Classifications of related propulsion mechanisms

		Travelling Wave	Stationary Wave
Electric actuated	PD	Toroidal mechanism [11, 14, 15]	Earthworm robot[6], multi-leg robots[22–26], PD-I*,PD-II*
	PL	Screw driven vehicle[17, 20], Thes-I[29]	Centipede robot[21], spiral wave[28] PL-I*
Hydraulic/ pneumatic actuated		Toroidal mechanism[12, 13]	Earthworm robot[7], inchworm robot[8], Bari-Bari-II[27]

* Mechanisms introduced in this thesis

Table. 2.2.1 shows a summary of the classification above. A PL type mechanism with stationary wave is considered more preferable for a watertight mobile robot for inspection in narrow space. In this table, the centipede robot and the spiral wave robot was classified to this category. However, the centipede robot generated wave motion by its legs, thus there were exposed rotating shaft and it was not belong to surface wave. The spiral wave robot had a propulsive surface, but

its internal rotating shaft was sliding through the external surface all the time, the friction may cause energy lost.

2.3 Purpose of this Research

In this research, we are interested in the stationary wave mechanism with electric actuation. To accomplish the concept of Surface Wave Mechanism, we have been conceiving a proper mechanical design, and three different prototypes, PD-I, PD-II and PL-I have been proposed in this research. Surface Wave Mechanism PD-I and PD-II can be classified to perpendicular type and Rotary Surface Wave Mechanism PL-I is parallel type as shown in Table. 2.2.1.

2.4 Chapter Summary

This chapter introduced several different types of propulsion mechanisms which generates wavy motion or has a propulsive skin. Then, the classification based on the characteristics of the mechanisms was proposed. Regarding to the features of each type, a PL type mechanism that generate stationary surface wave is considered to be suitable for watertight mobile robots in narrow space. But this type of mechanism has not been developed yet. Therefore, in the following chapters, we will first introduce the development of surface wave mechanism with stationary wave, and then focus on the PL type mechanism in particular.

Chapter 3

Development of Perpendicular Type Surface Wave Mechanism

3.1 Surface Wave Mechanism PD-I

3.1.1 Concept

The basic concept of Surface Wave Mechanism PD-I is shown in Fig. 3.1.1. The rubber pad connects to the motor through an eccentric cylinder and bearings. There is a small offset ΔX between the center of the rotating shaft and the center of eccentric cylinder. The eccentric distance causes vibrating motion when the motor is driven. Fig. 3.1.2 shows a cycle of the motion. The blue circle indicates the shaft of motor. When the motor shaft is driven clockwise, the rubber pad also makes a small scale rotating motion clockwise. Every time the rubber pad contacts the ground as shown in Fig. 3.1.2(3), due to the friction force between the contact surface and the ground, the mechanism moves a little to the right. The main idea of Surface Wave Mechanism PD-I was to make use of this vibrating motion to propel the mechanism.

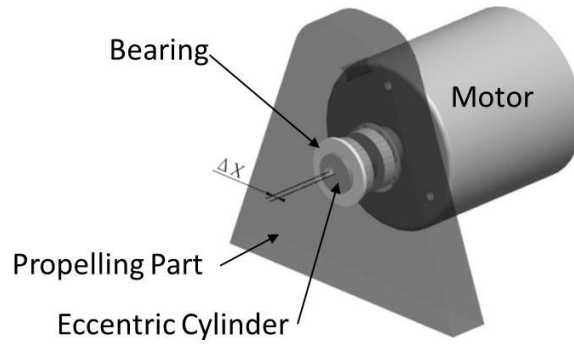


Fig. 3.1.1: Design concept of PD-I

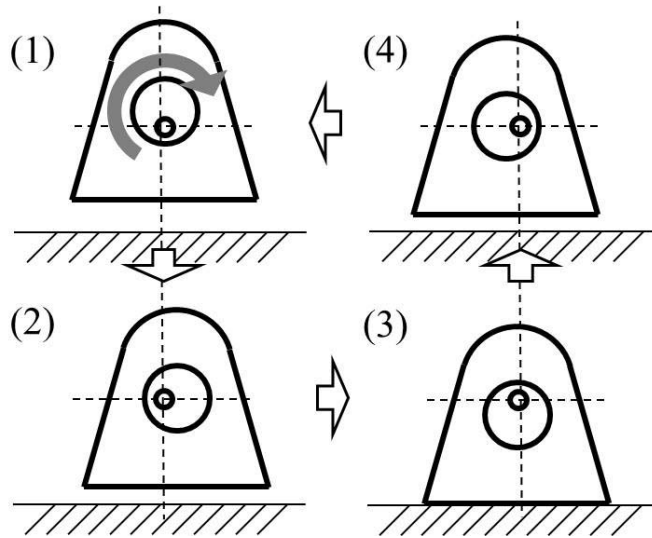


Fig. 3.1.2: Rotating motion caused by eccentric cylinder

3.1.2 Mechanical Design

To testify the concept of Surface Wave Mechanism PD-I, an experiment model was designed. Fig. 3.1.3 presents the overview of Surface Wave Mechanism PD-I. There were rubber pads on both left and right side of the mechanism, which were connected together by a frame at the bottom. An eccentric cylinder was inserted into the hole with bearings on one of the rubber pads. The shaft of the motor was inserted into

the eccentric hole on the cylinder. There was a 0.5mm offset between the center line of the cylinder and the center line of the eccentric hole. The specifications of Surface Wave Mechanism PD-I are shown in Table 3.1.1.

When the motor was driven, both of the rubber pads made small scale rotating motion due to the eccentric distance of the cylinder. As the explanations in previous section, this rotating motion could produce propulsion force and propel the mechanism.

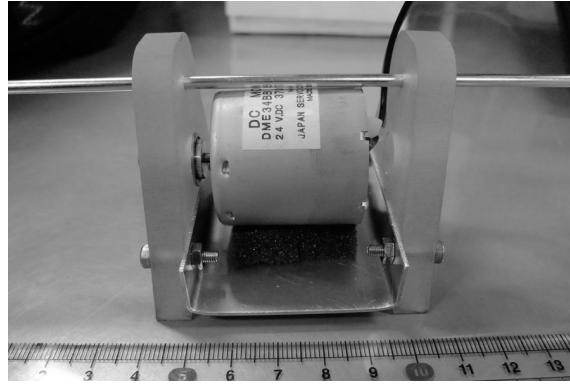


Fig. 3.1.3: Structure of PD-I

Table 3.1.1: Specifications of PD-I

Dimensions	$60\text{mm} \times 64.8\text{mm} \times 55\text{mm}$
Weight	180g
Actuator	DC 4.5 W
Weight of motor	110g

3.1.3 Experiment and Result

The mobility of Surface Wave Mechanism PD-I was tested by experiment. Fig. 3.1.4 shows images taken during the motion experiment. In this figure, the mechanism

moved to the left side but made turning motion in the meanwhile. A series of experiments were carried out, and the results showed that the performance of Surface Wave Mechanism PD-I was unstable. The expected motion of this mechanism was moving toward a certain direction corresponding to the rotational direction of the motor. However, when the mechanism was driven, it sometimes made turns and sometimes just vibrated at the same position. Thus, the mobility of Surface Wave Mechanism PD-I was not good.

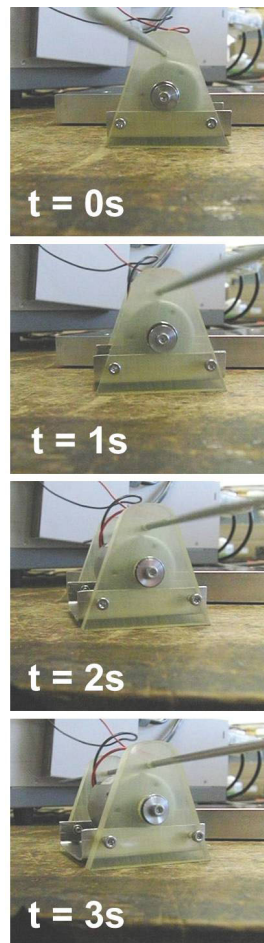


Fig. 3.1.4: Motion experiment of PD-I

3.1.4 Review and Modification

There were several possible reasons that might cause the unstable performance of Surface Wave Mechanism PD-I. First, the mechanism was driven by single motor on one side. This might have led to imbalance on both sides of the mechanism and caused turning motion. Second, the rubber pads did not keep in upright position while the mechanism was driven. Thus, the bottom surfaces of the rubber pads did not always contact the ground with the entire surface but sometimes hit against the ground with only left or right peak as sketched in Fig. 3.1.5. This might have caused reacting forces from various directions which interfered with the locomotion of Surface Wave Mechanism PD-I. Third, the motor used on Surface Wave Mechanism PD-I was quite heavy for the size of the mechanism. It might have caused difficulties in propulsion.

Considering these problems mentioned above, a modified model of Surface Wave Mechanism PD-I was designed. There were some principle points of this modification. Firstly, left side and right side of the modified model were symmetric to the central line. Secondly, the contact part of the mechanism changed from surface contact to point contact as shown in Fig. 3.1.6. This could make sure the contact area was consistent in every rotational cycle. Thirdly, a smaller motor was chosen for the modified model.

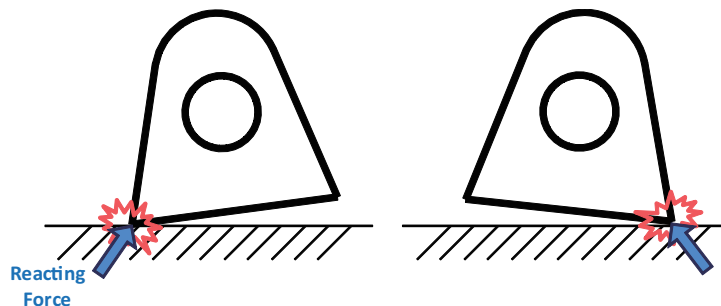


Fig. 3.1.5: Inclinations of rubber pads cause unsteadiness

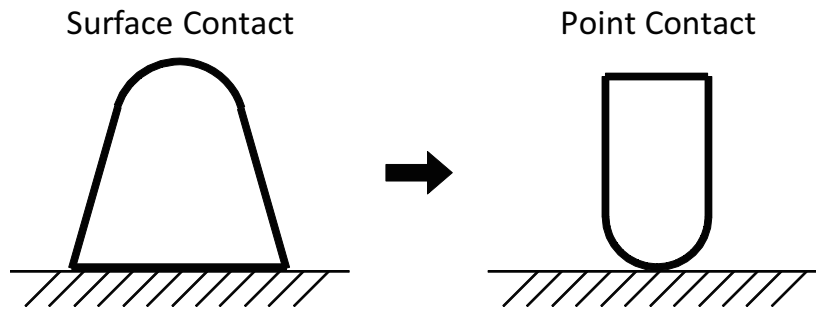


Fig. 3.1.6: Modification of contact part

The overview of modified Surface Wave Mechanism PD-I is presented in Fig. 3.1.7. Since the contact points were changed from surface contact to point contact, four legs were needed in order to keep the mechanism stable. There were four motors drive the four legs respectively. Table 3.1.2 shows the specifications of modified Surface Wave Mechanism PD-I. The motor used on this model was much smaller and lighter than the one on the previous model. AS same as the first prototype, the shafts of motors were inserted into eccentric cylinders which were mounted on the legs along with bearings. The contact points at the bottom of the legs were round shape as shown in Fig. 3.1.8. In order to keep the legs in upright position, at the top of each leg there was a pin-in-a-slot joint connecting to the main frame of the mechanism. Different from the previous model, the contact parts at the bottom of the legs was separate from the leg parts. Thus, the shapes or materials of the contact points were changeable in the later experiments.

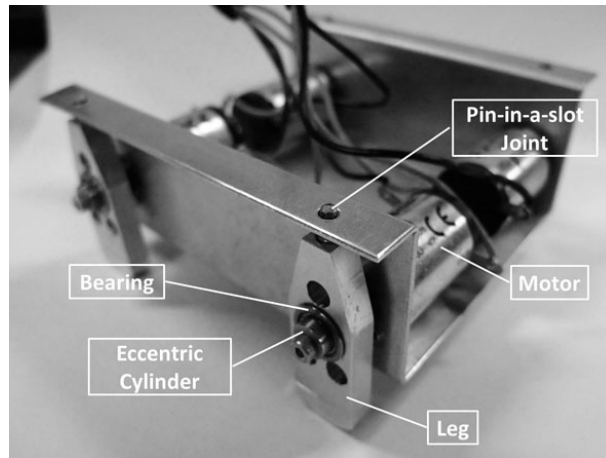


Fig. 3.1.7: Structure of modified PD-I

Table 3.1.2: Specifications of modified PD-I

Dimensions	80mm × 78mm × 40.5mm
Weight	343.5g
Actuator	Maxon, DC 2 W × 4
Weight of motor	21g × 4

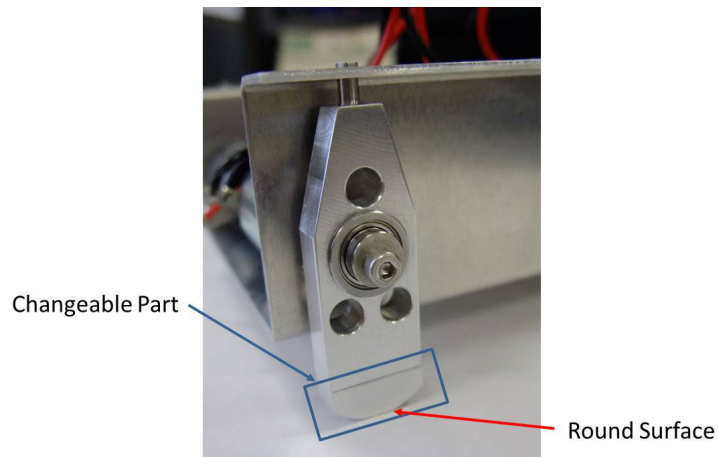


Fig. 3.1.8: Structure of the legs of modified PD-I

3.1.5 Experimental Result of the Modified Model

An experiment for the modified Surface Wave Mechanism PD-I was carried out. In this experiment, the four motors were driven together, and the performance of the mechanism was examined. Figure 3.1.9 shows the motion of modified Surface Wave Mechanism PD-I during the experiment. This experiment proofed that Surface Wave Mechanism PD-I could produce propulsive motion successfully, the proceeding speed was $108.7mm/s$ when the rotational speed of the motor was about $5200rpm$.

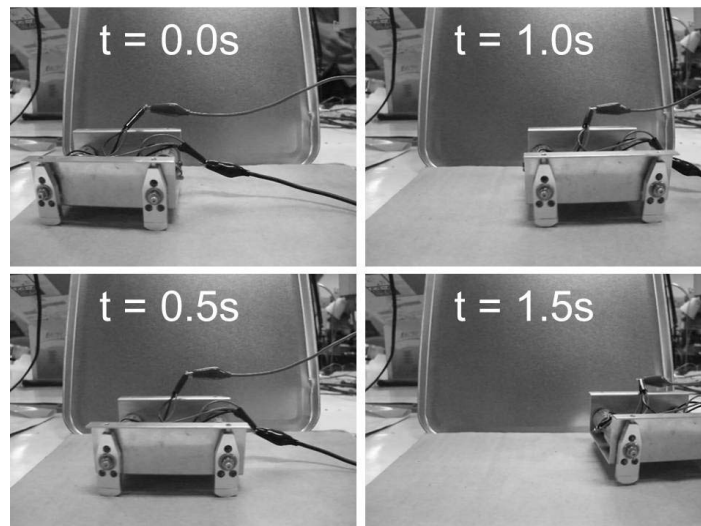
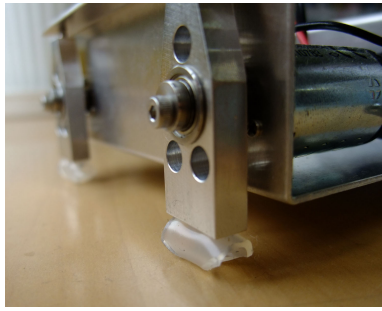
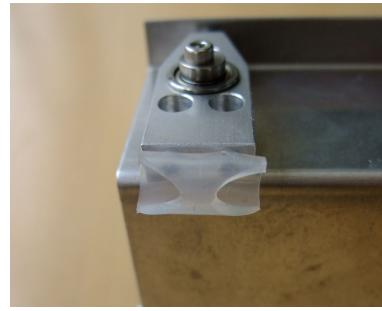


Fig. 3.1.9: Motion Experiment of modified PD-I

Nevertheless, the motion of this mechanism was not ideal. Sometimes the trail of its moving motion formed a curve but not a straight line. Surmising that the instability might have been caused by too strong vibrating motion, a partial modification was done. As shown in Fig. 3.1.10, the contact parts were changed to flexible material in order to absorb some of the impact. But experiments showed that this could not improve the performance. The moving direction of modified Surface Wave Mechanism PD-I was still unsteady.



(a) Overview



(b) Close-up view

Fig. 3.1.10: Modification of contact point

3.1.6 Discussion

Surface Wave Mechanism PD-I did not use any gear-head and the structure is very simple. The mechanism was vibrating and could generate propulsive motion. This prototype was not yet covered, but it can be covered by rubber sheet and becomes waterproof easily. The high speed vibration made the mechanism unstable and its proceeding direction was difficult to control, but still this kind of mechanism can be useful for reducing friction.

It might be an interesting study to improve the performance by adding encoders and synchronize the four legs with different gaits. But then the structure of the mechanism becomes more complicated. Since one of the original intentions of this research was to build a mechanism with simple structure, it is better to modify the mechanism in other ways.

3.2 Surface Wave Mechanism PD-II

3.2.1 Concept

Surface Wave Mechanism PD-I had testified the small scale rotating motion can produce propulsion forces. But at the same time it revealed that it is hard to keep steady moving direction if all the propelling legs were not synchronized. Besides, according to the results of previous models, high rotating speeds tend to cause strong vibration and cause unstable moving directions. Considering the problems above, Surface Wave Mechanism PD-II was designed. The main feature of Surface Wave Mechanism PD-II was utilizing crankshaft. An image of crankshaft is sketched in Fig. 3.2.1. When the shaft rotates along the axis, the crank pin a , b , and c all rotate and make circular trajectories with radius r . In this case, if three propelling legs are attached to the crank pin a , b , and c respectively, it is assured that the three legs rotate in the same rotation rate and keep constant phase differences between each other. In a word, a crankshaft can generate rotating motions as well as being a connecting part between different propelling legs. And this concept was applied to the design of Surface Wave Mechanism PD-II.

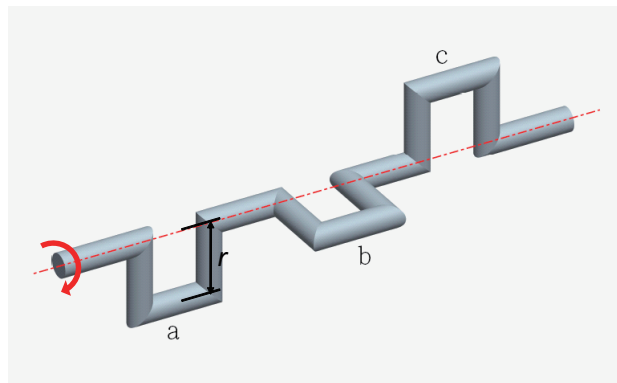


Fig. 3.2.1: Crankshaft

3.2.2 Mechanical Design

Figure 3.2.2 shows the structure of the mechanism. The left side and the right side of the mechanism were symmetric to the center. Two motors drove the two sides respectively. The power of motor was transmitted to a crankshaft through timing belt. Each of the crankshafts had three crank pins that were divided equally to the rotational axis. That is to say, there were 120 degrees phase differences among the pins. The propelling legs were designed to be sled-shape. Both of the front and rear parts of each leg were mounted to the crank pins with bearings. Thus, when the crankshaft was driven, the legs made rotating motions while keeping upright positions all the time.

In order to insert the legs into the crank pins, the crankshafts were designed as a series of circular plates and small pins as shown in Fig. 3.2.3. Each plate had two holes that were $3mm$ away from the center, and the included angle was 120 degrees. The small pins were fixed to the holes on the plates, and the plates were assembled to the frames on the main body with bearings. Thus, when one end of the crankshaft was driven by motor, the whole parts rotated together.

Appearance of Surface Wave Mechanism PD-II is shown in Fig. 3.2.4 (uncovered). And Table 3.2.1 is the specifications of this mechanism.

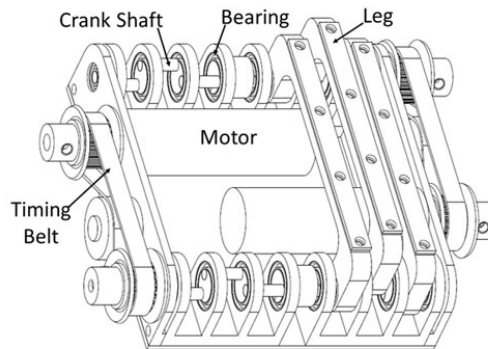


Fig. 3.2.2: Structure of PD-II

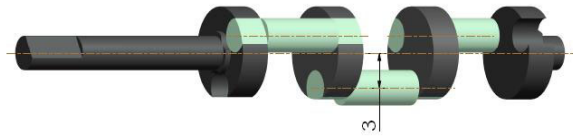


Fig. 3.2.3: Crankshaft of PD-II



Fig. 3.2.4: Bottom view of PD-II

Table 3.2.1: Specifications of PD-II

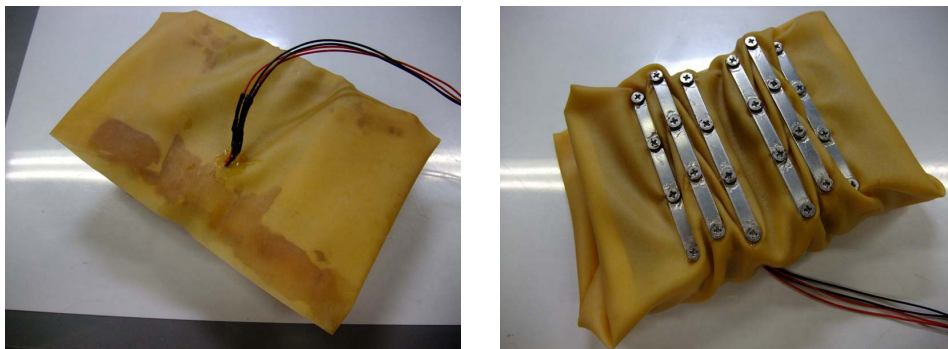
Dimensions	$80mm \times 109.6mm \times 38.4mm$
Weight	133.4g
Actuator	Canon, DC 3.1 W, Gear ratio 20 : 1 \times 2

3.2.3 Watertight Design

One of the main features of Surface Wave Mechanism is that it can be sealed against water and dust easily. In order to verify this characteristic, an underwater experiment was carried out. First of all, watertight device was mounted to the body of Surface Wave Mechanism PD-II.

The watertight device of Surface Wave Mechanism PD-II was simple. The whole body of the mechanism was wrapped up by a watertight rubber sheet. Fig. 3.2.5 shows the appearance of Surface Wave Mechanism PD-II after watertight device was mounted.

The sheet covered this mechanism entirely and was sealed by waterproof adhesive at every joint area. At the bottom of the mechanism, rubber sheet was clamped between the feet and plates as shown in Fig. 3.2.5b. Between every two feet, certain area of rubber sheet was reserved so that the strength of rubber did not interfere with locomotion.



(a) Top view

(b) Back

Fig. 3.2.5: Watertight design of PD-II

3.2.4 Motion Experiment

A series of experiments for evaluating the performance of Surface Wave Mechanism PD-II was carried out. The results showed that this mechanism could move steady and achieve basic motions such as moving forward, moving backward, and making turns. The sled-shape legs expanded the ground contact area and thus allowed the mechanism to move steady. Fig. 3.2.6 shows the moving motion of Surface Wave Mechanism PD-II.

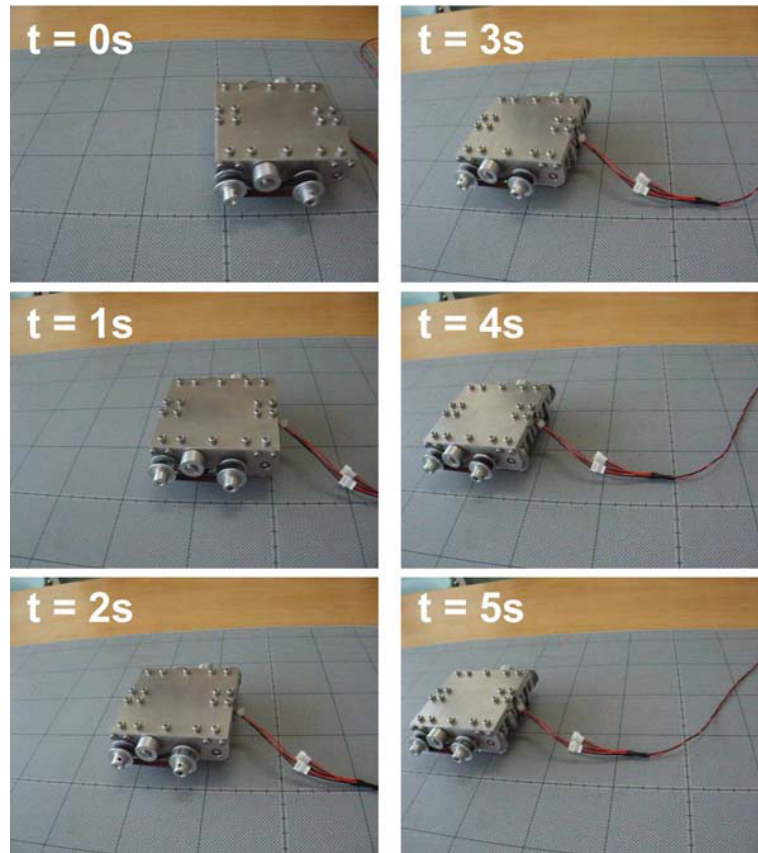


Fig. 3.2.6: Motion experiment

The proceeding speed of Surface Wave Mechanism PD-II under different rotational speed were measured, and the result is presented in Fig. 3.2.7. The line indicates the theoretical speed which was calculated from the specification of the motor and the dimensions of the model. The rotating velocity of the motor at 24volt was 430rpm, and the step length for each leg was $3\sqrt{3}$, thus the maximum velocity was about 111.7mm/s at 24volt. The speed is proportional to the supplied voltage theoretically. The triangle marks represents the speed of the mechanism before being covered by rubber sheet, and the round marks are the speed of the mechanism that was wrapped by rubber sheet. As expected, the proceeding speed of Surface Wave Mechanism PD-II increased along with the supplied voltage due to the increasing rotational speed of the motor. However, the experimental data was

not linear when the supplied voltage is high. One of the reasons might be slippage occurs more easily when the mechanism moves fast. The speed of the mechanism decreased after it was covered by rubber sheet. In addition, the minimum required power to drive the mechanism became higher. This might due to the elastic force of rubber sheet. The elastic force caused resistance during the propelling motion of Surface Wave Mechanism PD-II. As a result, the mechanism needed more power to reach the same speed.

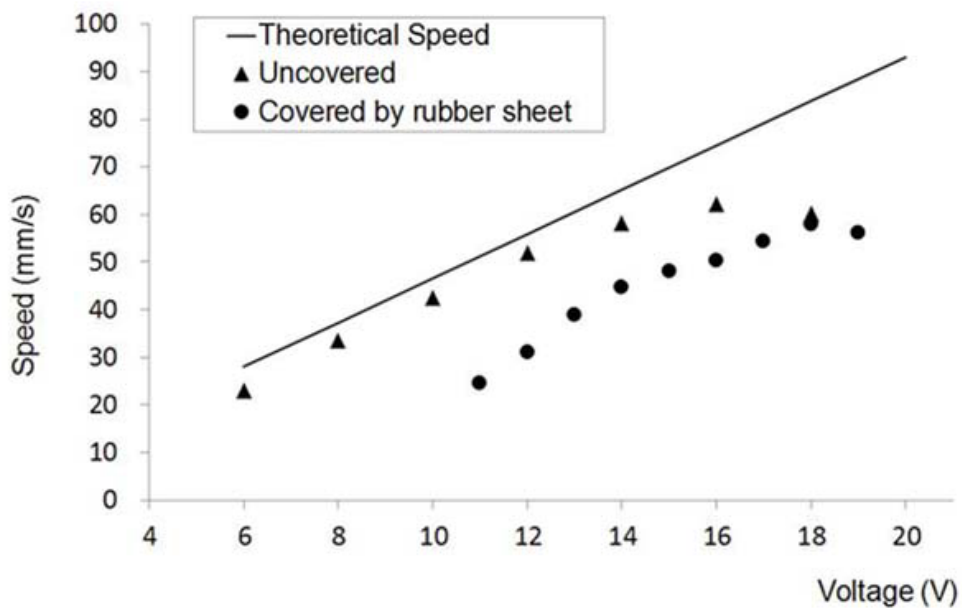


Fig. 3.2.7: Proceeding speed of PD-II

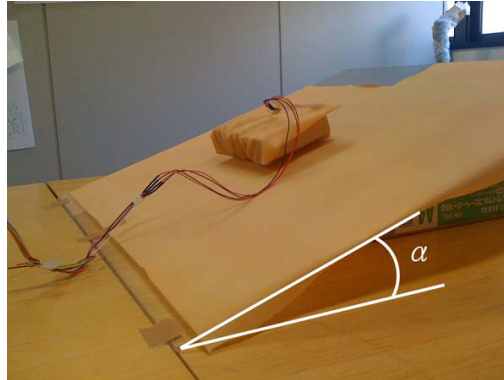


Fig. 3.2.8: Slope climbing experiment

In another experiment, the prototype of Surface Wave Mechanism PD-II was put on a slope to test its climbing ability. The slope was made by an acrylic board and sheeted with a rubber sheet as shown in Fig. 3.2.8. The inclination of the slope was changed from small to large until the mechanism could not climb up any more and the maximum angle was recorded. According to this experiment result, Surface Wave Mechanism PD-II could climb up slopes under 17 degrees inclination angle. Nevertheless, the climbing ability depends on the friction, the result may change in other environment.

3.2.5 Underwater Experiment

After watertight device was mounted, an underwater experiment was carried out on Surface Wave Mechanism PD-II. There were two purposes of this underwater experiment. One was to verify that the watertight device sealed against water properly; the other was to prove that this mechanism performs good mobility underwater.

Fig. 3.2.9 shows the image taken during this experiment. Surface Wave Mechanism PD-II was put into a water tank. The depth of water was just about the same height with the mechanism. More water was not filled because the weight of Surface Wave Mechanism PD-II could not counteract with the buoyancy. During

the experiment, Surface Wave Mechanism PD-II was driven underwater for one and a half hour, and some basic motions were tested including moving forward, moving backward and making turns.

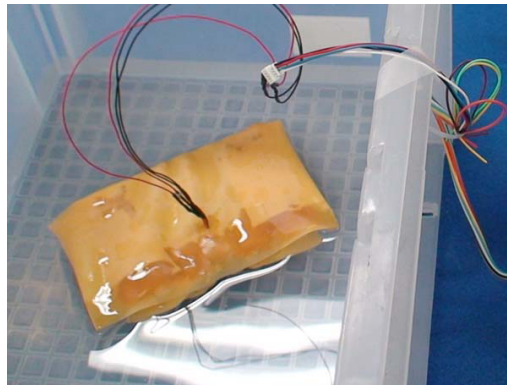


Fig. 3.2.9: Watertightness experiment

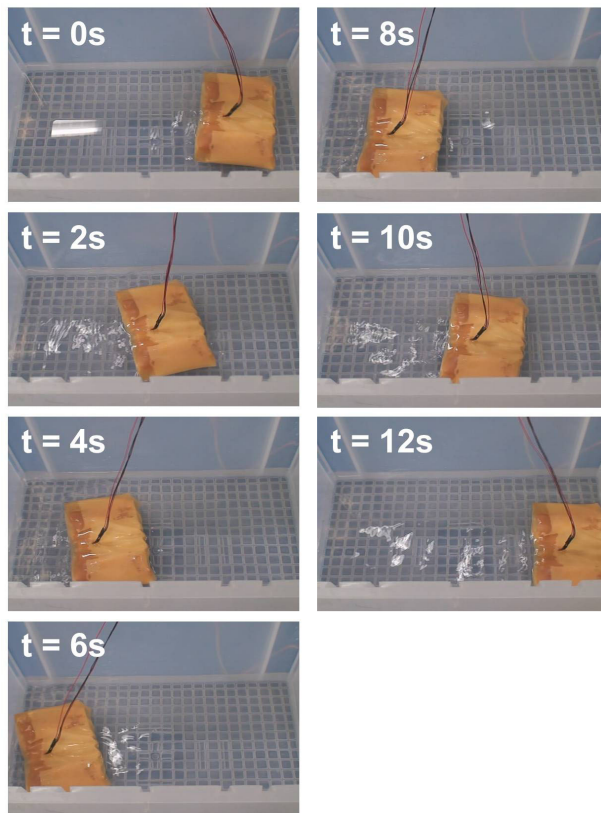


Fig. 3.2.10: Top view of underwater experiment

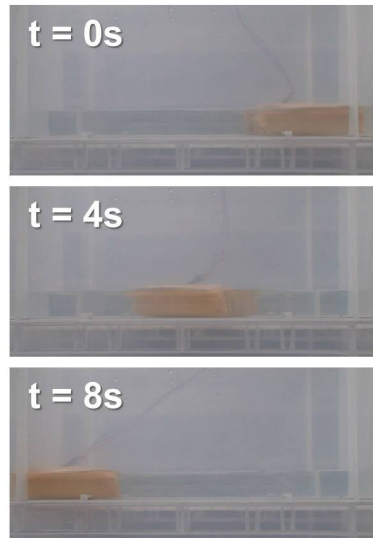


Fig. 3.2.11: Side view of underwater experiment

The result of underwater experiment showed that Surface Wave Mechanism PD-II was completely watertight and could operate underwater well. Basic motions such as moving forward and backward, making turns were also accomplished successfully. Fig. 3.2.10 shows top view images that the mechanism moving forward and backward in the water. And side view of the motion is shown in Fig. 3.2.11.

3.2.6 Discussion

Surface Wave Mechanism PD-II showed mobility with good maneuverability and water-tightness. However, both Surface Wave Mechanism PD-I and Surface Wave Mechanism PD-II have only a single propelling surface. If they are turned over in the rough terrain, they could not function any more. Thus, it is better to have propelling parts on every surface of the mechanism. To solve this problem, one possible solution is to combine three units of Surface Wave Mechanism PD-II to form a triangle in cross-section as shown in Fig. 3.2.12, but the vehicle then becomes rather complex and heavy.

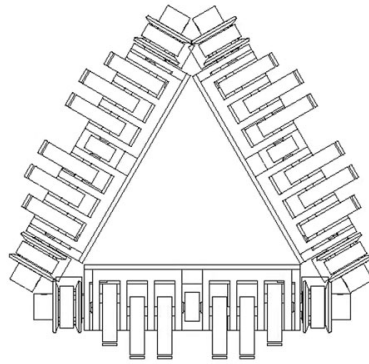


Fig. 3.2.12: Image of triangle structure

3.3 Chapter Summary

In this chapter, two different PD type surface wave mechanisms were introduced. Starting from the concept, then the mechanical design, and finally the experimental results were explained. To summarize, Surface Wave Mechanism PD-I generates vibration for locomotion, but the performance of the prototype showed that its propulsive motion was unsteable. On the other hand, Surface Wave Mechanism PD-II uses crank shaft to generate steady propulsive motion, and it is sealed against water entirely.

Both of the two models have only a single propulsive surface. To improve the mobility, we would like to develop another mechanism with larger propulsive surface in the next step.

Chapter 4

Development of Parallel Type Surface Wave Mechanism

4.1 Concept

As mentioned in section 2.2, most of the existing propulsion mechanisms with stationary wave are PD type. PL type that generate wave motion parallel to the rotating shaft is relatively rare. What we want to develop is the device which generates stationary wave motion toward axial direction by the rotation of central axis. To produce this specific motion, we would like to introduce a brand-new mechanism, Rotary Surface Wave Mechanism PL-I.

The main component of Rotary Surface Wave Mechanism is shown in Fig. 4.1.1. It is a round disc fixed on a shaft with an inclination ϕ and an eccentricity ε . When the shaft is rotated, the rim of the eccentric inclined disc generates rotating motions as shown in Fig. 4.1.2. Fig. 4.1.2(1) shows four different positions during one rotation cycle. Each of the adjacent disc in the figure has a 90 degrees phase shift. O_1, O_2, O_3 and O_4 are the eccentric rotating centers of the disc. $a_1, a_2, a_3,$ and a_4 are the topmost points of the disc at a moment in time. And b_1, b_2, b_2, b_2

are the bottommost points of the disc at the same moment. By connecting a_1 to a_4 and b_1 to b_4 in order, the trails for the rim of the disc are generated as shown in Fig. 4.1.2(2). Each trail forms an irregular circular shape.

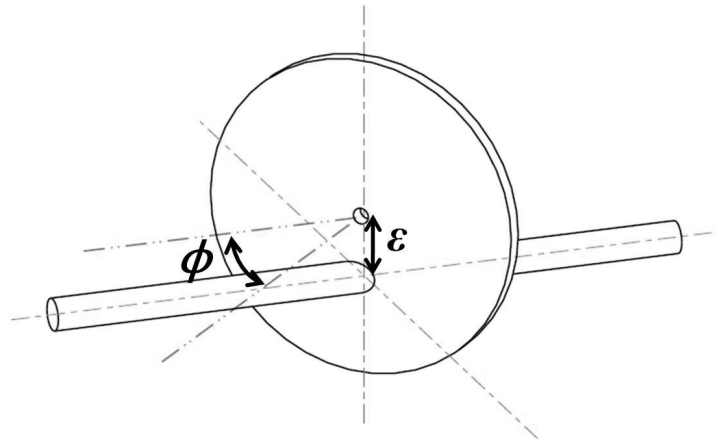


Fig. 4.1.1: Eccentric inclined plate

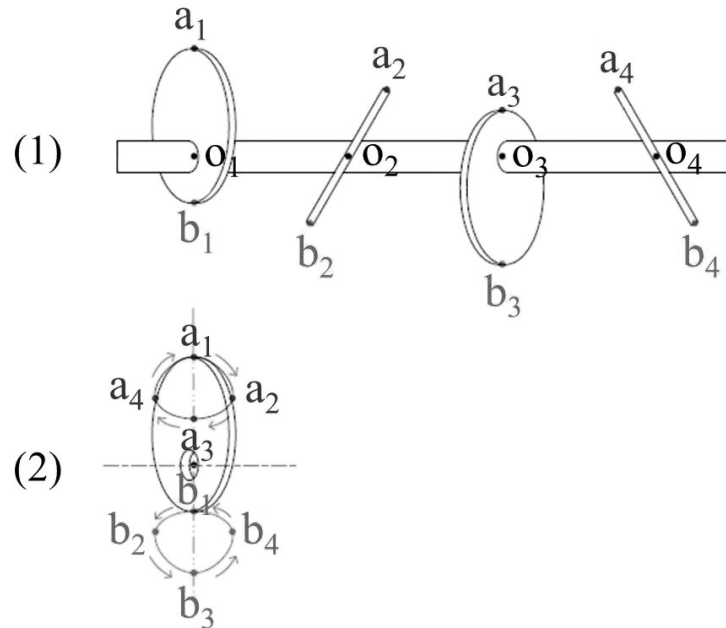


Fig. 4.1.2: Rotating motion generated by the rim of eccentric inclined disc

The trail of the upper rim is counter-clockwise, while the one of lower rim is clockwise. By properly applying this motion to a mechanical device, these circular trails can generate propulsion force and make the device move. This is the basic concept of Rotary Surface Wave Mechanism. It should be noted that this mechanism is axially symmetric. Thus the same propulsive motion is generated in all directions radially from the rotating axle, which assures that the mechanism can keep functioning regardless of its upright position.

4.2 Motion Analysis and Simulation

In order to testify the above-mentioned motion theoretically, the motion of the disc was analyzed by using vector analysis.

Define the z -axis as the rotating axle. C_1 is a circle with radius r on the xy -plane and centered at the origin of the coordinates as shown in Fig. 4.2.1. The vector \mathbf{P}_1 on C_1 can be written as:

$$\mathbf{P}_1 = \begin{bmatrix} r \cos \theta \\ r \sin \theta \\ 0 \end{bmatrix} \quad (4.2.1)$$

Rotate the circle C_1 along y -axis for an inclination ϕ to obtain the circle C_2 , which is also centered at the origin of the coordinates but has included angle ϕ with xy -plane along y -axis as shown in Fig. 4.2.2.

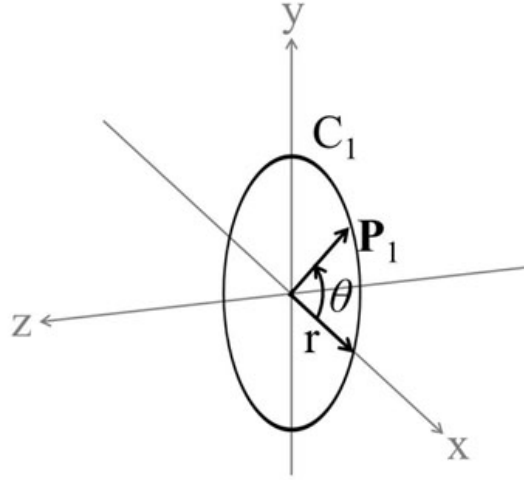


Fig. 4.2.1: Circle C_1 on xy -plane

$$\begin{aligned}
 \mathbf{P}_2 &= \begin{bmatrix} \cos \phi & 0 & \sin \phi \\ 0 & 1 & 0 \\ -\sin \phi & 0 & \cos \phi \end{bmatrix} \mathbf{P}_1 \\
 &= \begin{bmatrix} r \cos \theta \cos \phi \\ r \sin \theta \\ -r \cos \theta \sin \phi \end{bmatrix} \tag{4.2.2}
 \end{aligned}$$

Then, shift the circle C_2 along y -axis for an eccentric distance ε . The vector \mathbf{P}_3 on an eccentric inclined circle C_3 as shown in Fig. 4.2.3 is obtained.

$$\mathbf{P}_3 = \begin{bmatrix} r \cos \theta \cos \phi \\ \varepsilon + r \sin \theta \\ -r \cos \theta \sin \phi \end{bmatrix} \tag{4.2.3}$$

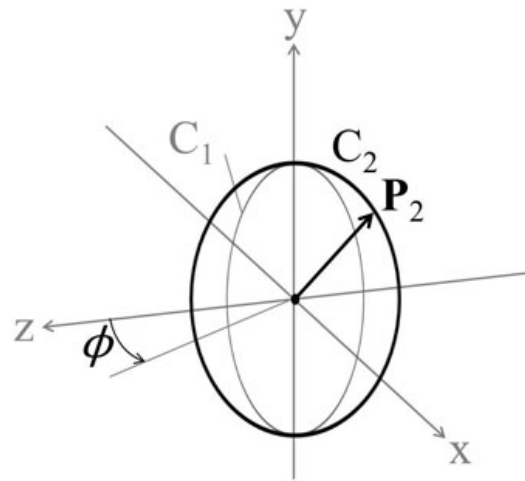


Fig. 4.2.2: Inclined circle C_2

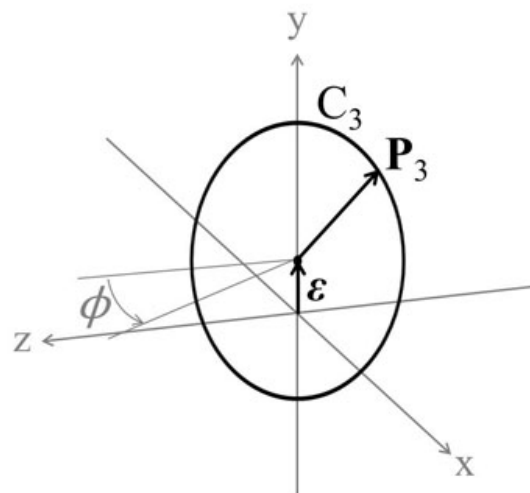


Fig. 4.2.3: Eccentric inclined circle C_3

Rotate C_3 along z -axis:

$$\begin{aligned}
 \mathbf{P} &= \begin{bmatrix} \cos \xi & -\sin \xi & 0 \\ \sin \xi & \cos \xi & 0 \\ 0 & 0 & 1 \end{bmatrix} \mathbf{P}_3 \\
 &= \begin{bmatrix} r \cos \theta \cos \phi \cos \xi - \sin \xi (\varepsilon + r \sin \theta) \\ r \cos \theta \cos \phi \sin \xi + \cos \xi (\varepsilon + r \sin \theta) \\ -r \cos \theta \sin \phi \end{bmatrix} \quad (4.2.4)
 \end{aligned}$$

To obtain the trajectory of the motion of the contact point, we need to obtain

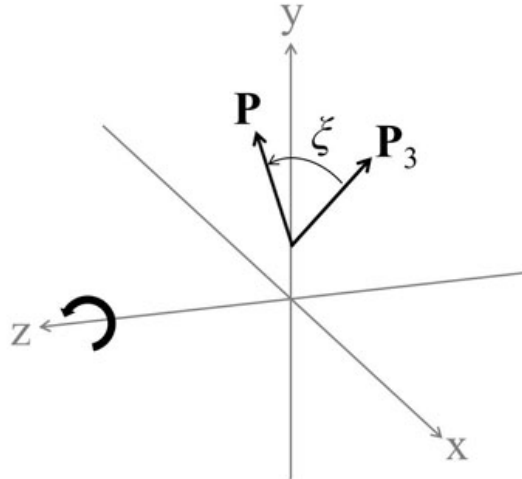


Fig. 4.2.4: Rotate \mathbf{P}_3 along z -axis

the lowest point on the circle at every rotating angle ξ . The lowest point occurs when \mathbf{P}_y has the minimum value at each rotating angle ξ . At the minimum point, $d\mathbf{P}_y/d\theta = 0$ must be true.

$$\frac{d\mathbf{P}_y}{d\theta} = -r \cos \phi \sin \xi \sin \theta + r \cos \xi \cos \theta = 0 \quad (4.2.5)$$

$$\cos \phi \sin \xi \sin \theta = \cos \xi \cos \theta \quad (4.2.6)$$

$$\sin^2 \theta (\cos \phi \tan \xi)^2 = \cos^2 \theta \quad (4.2.7)$$

$$\sin \theta = \frac{\pm 1}{\sqrt{(\cos \phi \tan \xi)^2 + 1}} \quad (4.2.8)$$

$$\theta^* = \sin^{-1} \frac{\pm 1}{\sqrt{(\cos \phi \tan \xi)^2 + 1}} \quad (4.2.9)$$

Substitute θ^* for the θ in Eq.(4.2.4), the contact point of the circle at every rotational angle ξ can be obtained.

Based on the result of the above analysis, a simulation was done by using Matlab. The code is included in Appendix B. In the simulation, ϕ , ε are given, and ξ is change from 0° to 360° in order to complete a rotation cycle. The simulation result is shown in Fig. 4.2.5. The thick circle indicates the eccentric inclined circle C_3 . The horizontal line indicates the rotating axle. When the circle rotates along the axle, its position changes as the circles drawn in thin lines on the figure. And the dashed line loops are the trajectories of the circle which are generated by connecting the lowest/highest points of C_3 during one rotation cycle. Fig. 4.2.6 shows the shape of the generated trajectory in three different views. The solid line is the drive phase, and the dotted line is the recovery phase of a stroke cycle. The simulation result proved that the rotating motion of an eccentric inclined circle generates circular trajectories on yz -plane, which is parallel to the rotating shaft. Thus, it is expected that this motion can be applied to the propulsion mechanism for generating propulsive forces. However, to see from the top view, in this case xz -plane, the drive stroke is not parallel to the z -axis. This may cause side way movement.

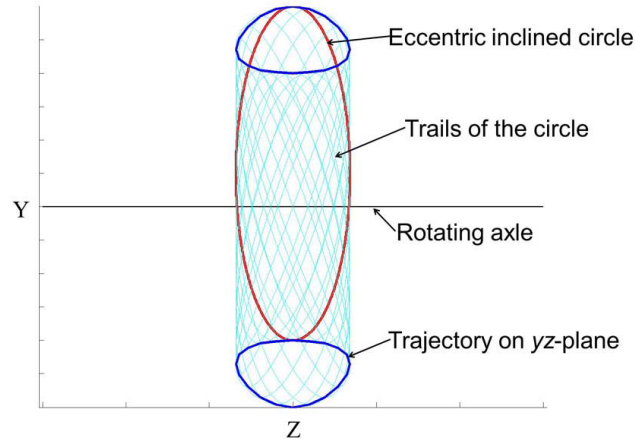


Fig. 4.2.5: Simulation result of Rotary Surface Wave Mechanism

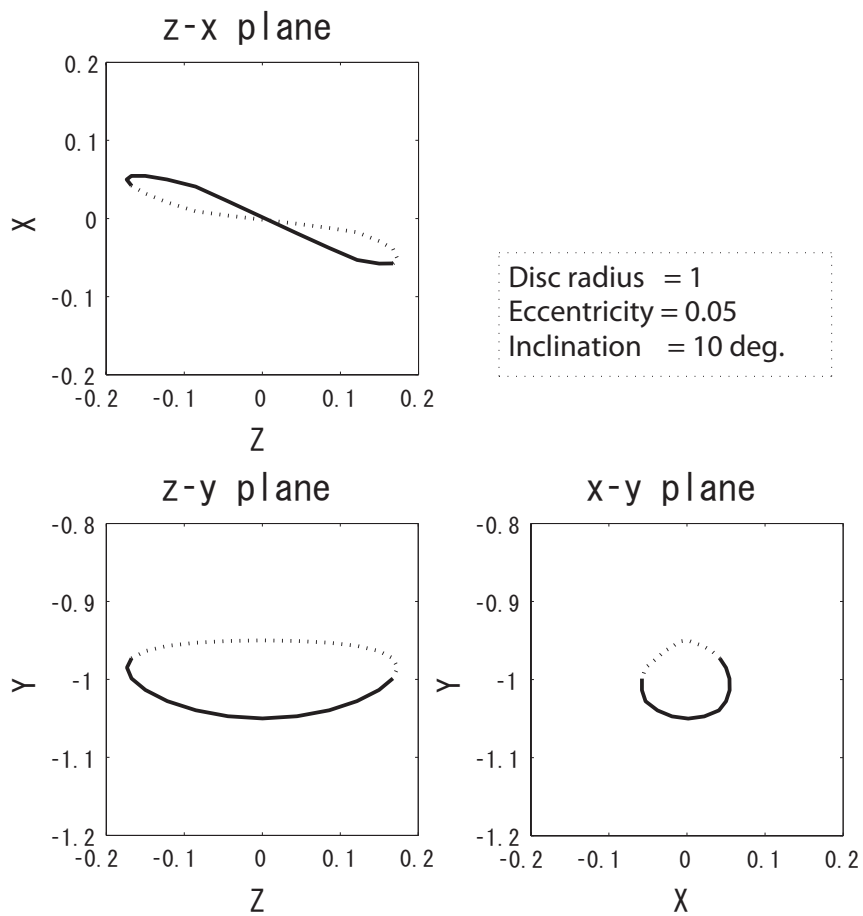


Fig. 4.2.6: Shape of the trajectory in different views

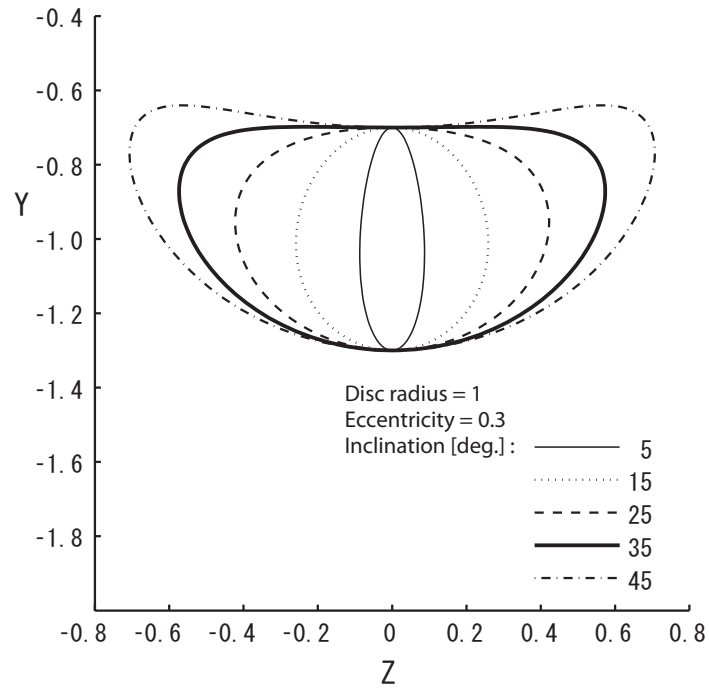


Fig. 4.2.7: Trajectory of different inclination

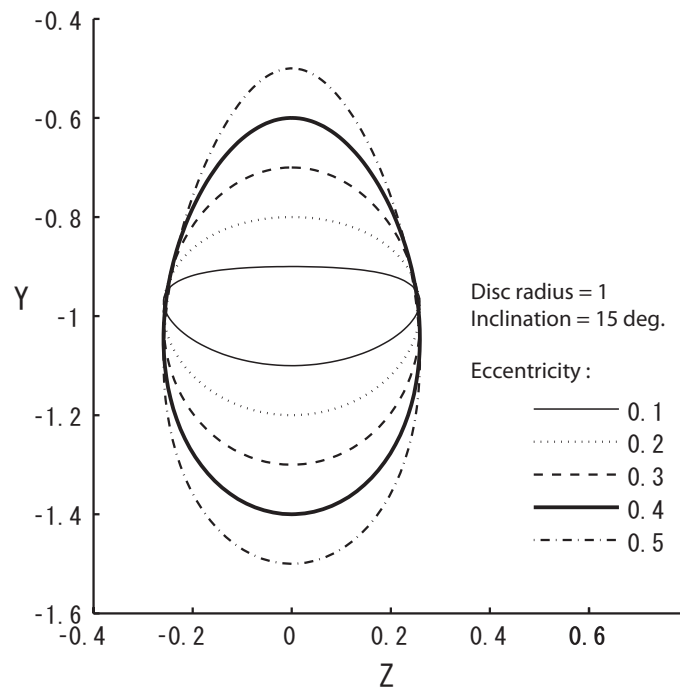


Fig. 4.2.8: Trajectory of different eccentricity

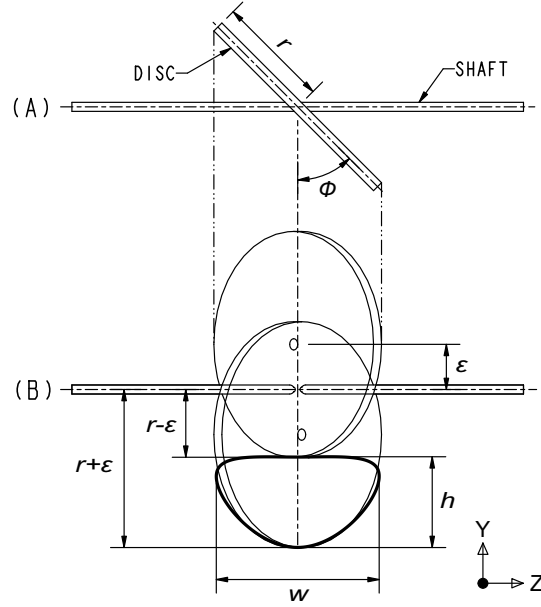


Fig. 4.2.9: Size of trajectory

As is easily assumed, the shape of the trajectories is affected by inclinations ϕ and eccentricity ε of the disc. In order to find out the effect of these variable, simulations were done with different values of ϕ and ε . Assume the radius of the disc, r , is 1, and ε is $0.3r$. When ϕ alters from 5 degree to 45 degree, the trajectory changes as shown in Fig. 4.2.7. When ϕ is fixed to 15 degree, and ε changes from $0.1r$ to $0.5r$, the trajectory changes as shown in Fig. 4.2.8. Basically, the inclinations ϕ affects the width w of the trajectory and the eccentric distances ε affects the height h of the trajectory. Fig. 4.2.9 shows a sketch of this relationship, and it can be represented as the following equations:

$$h = (r + \varepsilon) - (r - \varepsilon) = 2\varepsilon \quad (4.2.10)$$

$$w = 2r \sin \phi \quad (4.2.11)$$

Hence, a larger eccentricity would make the height of the trajectory larger, which is good for striding across obstacles on uneven terrain. Larger inclinations would

make the width of the trajectory wider, which means a longer stride length for each rotation cycle and better propulsion efficiency.

4.3 The First Prototype

4.3.1 Mechanical Design

Figure 4.3.1 shows the first prototype of Rotary Surface Wave Mechanism. It was basically composed of eight units of eccentric inclined disc, a rotating shaft, and a driving motor. Each eccentric inclined disc unit was mounted on the rotating shaft with a 90 degrees phase shift between adjacent discs, hence the eight units of inclined disc make two cycles of the rotating motion. This makes sure that there were at least two points in contact with the ground at any time.

The structure of one eccentric inclined disc unit is shown in Fig. 4.3.2. There was a disc with a hole with an eccentricity of $12mm$ and a 20 degrees inclination. This unit was fixed on the rotating shaft through the hole. The disc was surrounded by an outer ring which had four rubber feet made by urethane. There was a bearing between the disc and the outer ring. Thus, even though the central disc is fixed on the rotating shaft, the outer ring can rotate freely.

The whole rotating part of this mechanism was covered by rubber bellows as shown in Fig. 4.3.3. The bellows were mounted between each outer ring. There are two reasons for adding these bellows: Firstly, the bellows covered the mechanism and protected it from water and dust. Secondly, the bellows connected every outer ring and fixed to the frame on both ends. Bellows has the characteristic that it is flexible, easy to bend, but hard to twist. These bellows restrained the outer rings from rotation. As a result, while the eccentric inclined discs rotate along the shaft, the outer rings do not rotate simultaneously. Instead, the rotating motion of the eccentric inclined disc made the outer ring change its inclination and has some

displacement in the direction normal to the rotating shaft. The moving trail of each point on the outer rings formed a circular shape as explained in the previous section. Therefore, when the shaft was driven, all the rubber feet made small rotating motions and propelled the mechanism. Table 4.3.1 shows the specification of Rotary Surface Wave Mechanism.

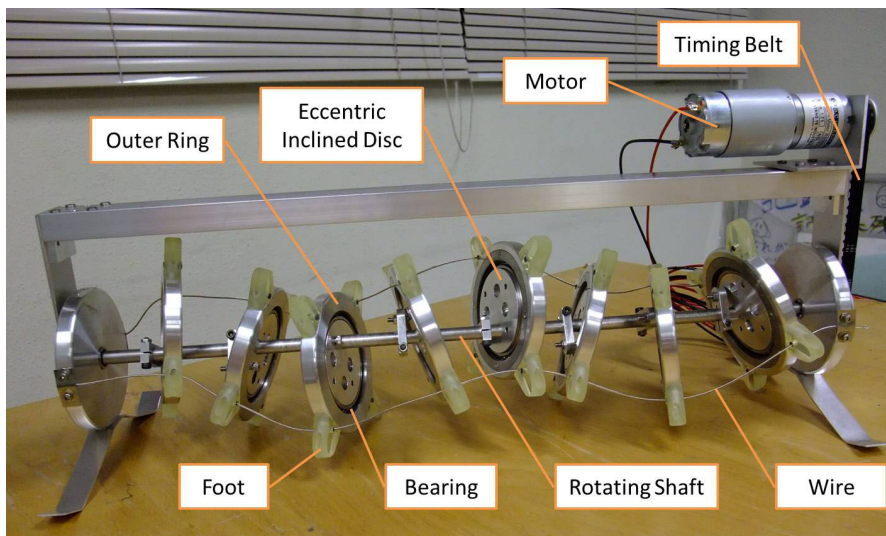


Fig. 4.3.1: Prototype of RS-Wave Mechanism

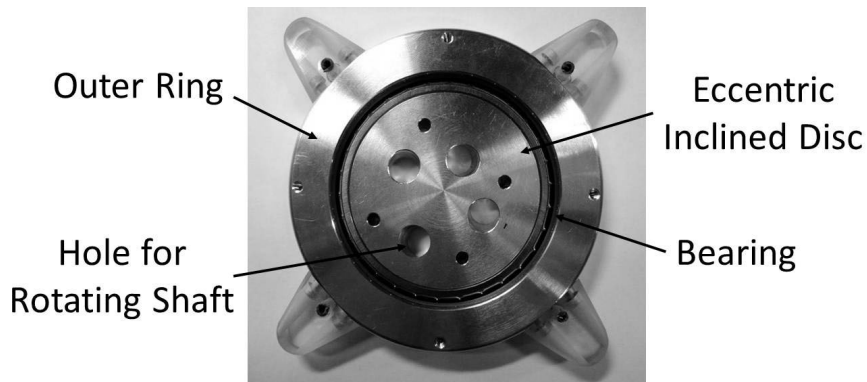


Fig. 4.3.2: Eccentric inclined plate unit

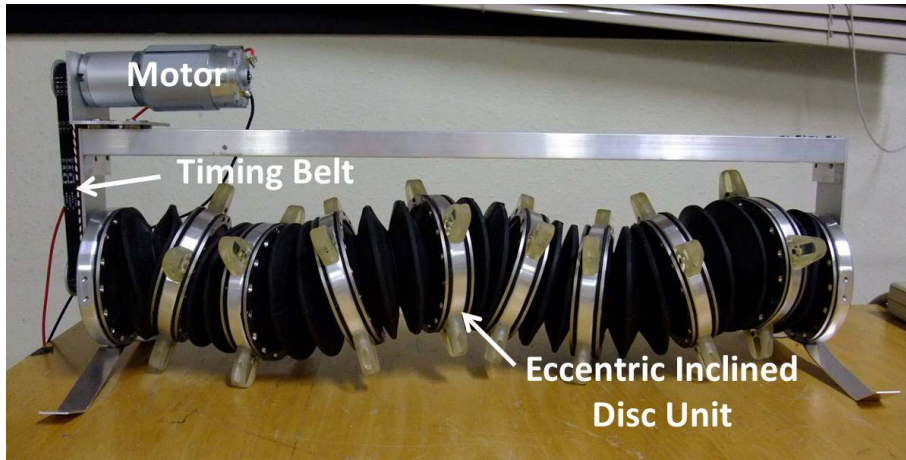


Fig. 4.3.3: Overview of RS-Wave Mechanism

Table 4.3.1: Specifications of the Prototype

Dimensions	$479.3mm \times 135.3mm \times 200.9mm$
Weight	$3.25kg$
Actuator	Mabuchi, DC 13.1W, Gear ratio 71 : 1

4.3.2 Experiment and Result

A basic motion experiment was applied to test the performance of Rotary Surface Wave Mechanism. In the experiment, Rotary Surface Wave Mechanism was put on a flat surface and the motor was driven. The motion generated by the mechanism was examined. Fig. 4.3.4 shows the motion of Rotary Surface Wave Mechanism. It was capable of making steady motion. This experimental result proved that Rotary Surface Wave Mechanism can generate propulsive motion successfully.

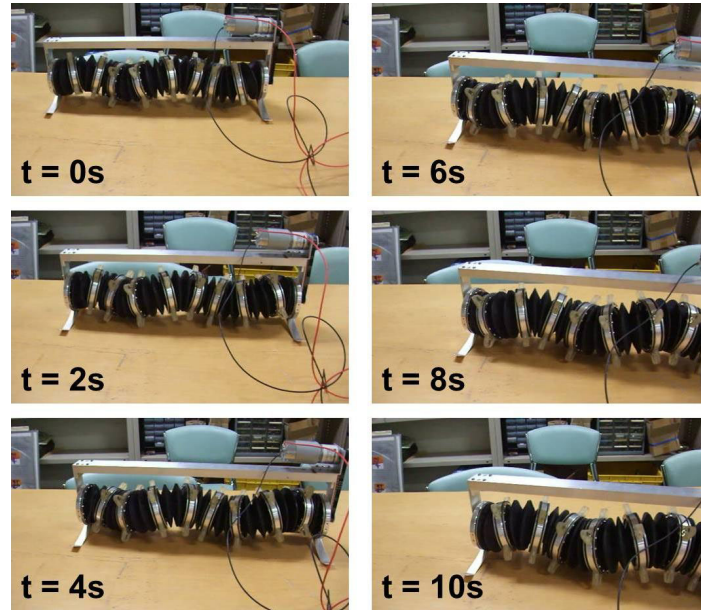


Fig. 4.3.4: Motion experiment

However, as what we noticed in the simulation result in Fig. 4.2.6, the moving direction of the mechanism was not parallel to the axial direction. There was an included angle of about 40 degree between the moving direction and the axial direction. The proceeding toward a deflected direction is unfavourable for the robot to enter narrow space.

4.3.3 Modification and Torque Measurement

Since the motion of Rotary Surface Wave Mechanism is mainly related to the inclination ϕ and eccentricity ε of the discs, it is essential to find out the optimal parameters. In order to adjust the inclination and eccentricity, the structure of the prototype was modified. All the eccentric inclined discs in the first prototype were replaced with new components as shown in Fig. 4.3.5. In the center of the component, there are two screws fixed in parallel. There is a block that can rotate in certain angle and slide along the screws, and it can be lock at certain position

by nuts. The rotating shaft passes through the blocks. With this adjustable components, we can change the inclination ϕ and eccentricity ε of the discs. In the experiment, the mechanism was assembled several times with different inclinations and eccentricity. The torque of the mechanism under operation was measured and recorded.

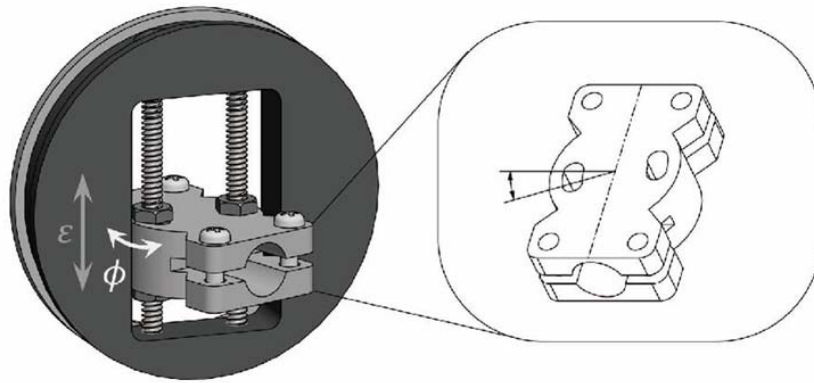


Fig. 4.3.5: Adjustable parts

The experiment result is shown in Fig. 4.3.6. The dashed line is the torque when the eccentric incline disc unit had an eccentricity ε of $3mm$. And the dotted line shows the torque when the ε was $6mm$. The inclination ϕ was set to 10, 15, and 20 degrees. The result shows the tendency that the torque of the mechanism increases when it has either larger eccentricity or larger inclination. However, when the value of ϕ and ε are small, the propelling speed is slow. Thus there is a trade-off on selection of design parameters.

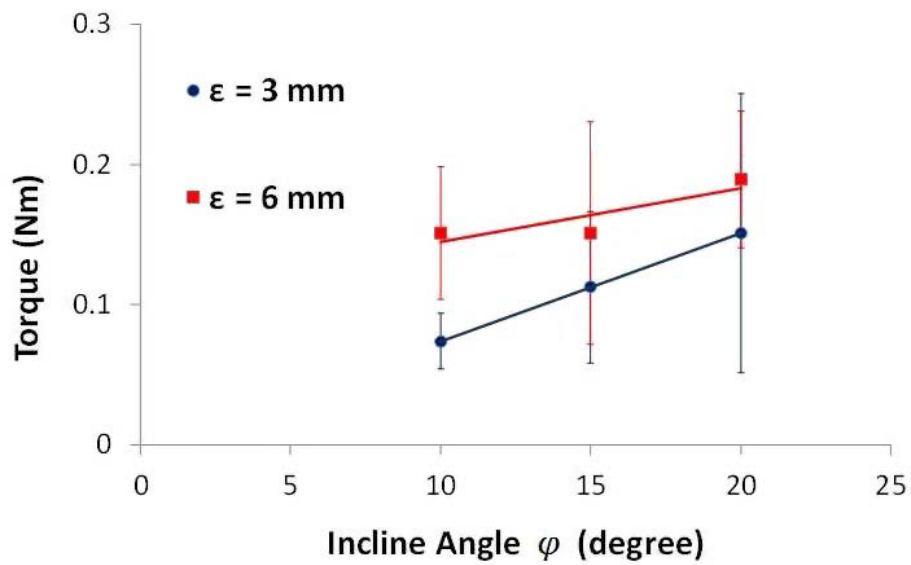


Fig. 4.3.6: Torque under different inclinations and eccentric distances

4.4 Chapter Summary

In this chapter, a parallel type surface wave mechanism called RS-wave mechanism was introduced. First, the principle of the mechanism was explained. Then, the propulsive motion was analyzed by mathematical model, and a motion simulation was conducted. After that, the first prototype was built and evaluated by experiment. Motion of the prototype was consistent with the design concept, RS-Wave mechanism generated smooth and steady propulsive motion. Finally, some important design parameters of RS-Wave mechanism were discussed.

Chapter 5

Development of RS-Wave Vehicle

5.1 Modification of RS-Wave Mechanism

The first prototype of RS-Wave mechanism was driven by a motor that was fixed on an exterior frame. For a better applicability, the design should be more compact and it is better to replace the exterior frame by an interior structure and a build-in actuator.

Figure 5.1.1 shows the modified structure of RS-Wave mechanism. The eccentric inclined discs are mounted on a rotating pipe instead of a rod. Inside of the rotating pipe, there is another pipe that connects the front and rear parts of the body. Inside the internal fixed pipe, the motor, motor driver and controllers are placed. The motor drives the external rotating pipe through a custom made planetary gear set, which is shown in Fig. 5.1.2. The sun gear is fixed on the output shaft of the motor, and an inner gear is fixed on the rotating pipe. There are two pinion gears that transfer the power from the motor to the inner gear. Besides the pinion gears, there are four fixed supports that connect the internal pipe with the front lid of the mechanism.

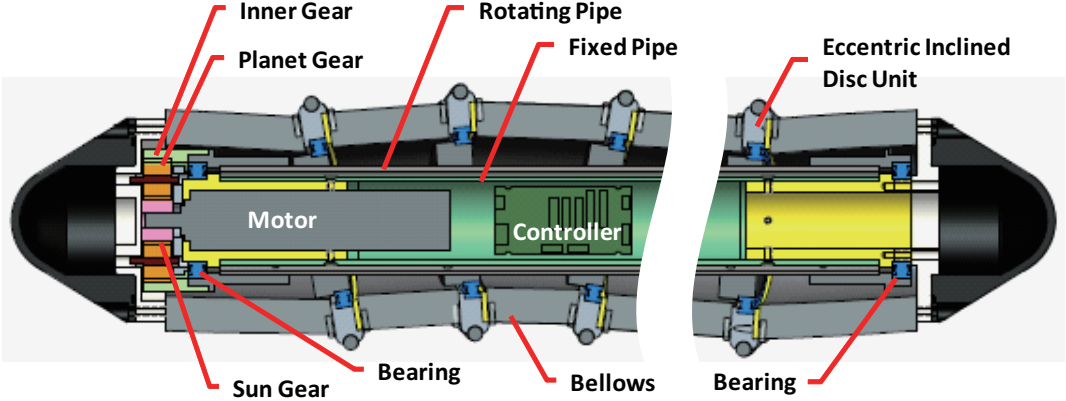


Fig. 5.1.1: Structure of RS-Wave unit

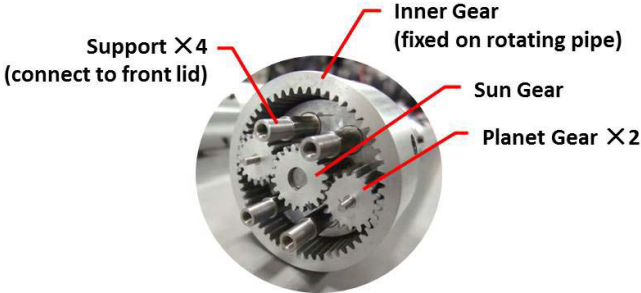


Fig. 5.1.2: Planetary gear set

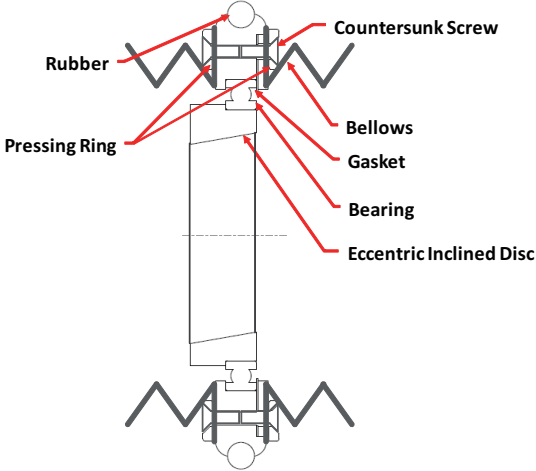


Fig. 5.1.3: Design of the eccentric inclined disc unit

Figure 5.1.3 shows the section view of one eccentric inclined disc unit. From the center, there are the eccentric inclined disc, a large bore bearing, and an external ring. The edge of the external ring which contact to the ground is covered by rubber. There are bellows between each disc unit that protect this mechanism from water and dust. To fix the bellows, there are pressing rings on both side of the external ring, rubber bellows are clamped between the rings.

The design parameters of the eccentric inclined disc units are shown in Table 5.1.1. The radius of each external ring is $44mm$, and the internal disc has an inclination of 10 degrees and an eccentricity of $3mm$. One RS-Wave unit has 8 eccentric inclined discs in series. The adjacent discs are separated by $50mm$ and have 90 degrees phase difference. Hence, the wave length generated by this RS-Wave unit is $200mm$. These parameters were decided regarding the size and energy efficiency. The space inside the internal pipe needs to be wide enough to accommodate sufficiently the motor and controllers. At the meanwhile, the total size of the robot is preferred to be miniaturized for locomotion in narrow space. Thus, small eccentricity and small incline angle of the disc were chosen. Besides, it also allows the mechanism not wasting much power on the resistance of bellow deformation. However, there is a trade-off that the robot is unable to run fast.

Table 5.1.1: Dimensions of eccentric inclined disc unit

Radius r	$44mm$
Inclination ϕ	10°
Eccentricity ε	$3mm$
Interval between discs	$50mm$
Phase shift between discs	90°

A simple kinematic simulation with these design parameters was conducted. The black circular loop in Fig. 5.1.4 is the trajectory of the lowest point on the disc during one rotation cycle. In four different phases, the discs will contact the ground

alternately; the period indicated in red is the period that each disc contacts to the ground and generating propulsion force. The stride length is 10.95mm . Therefore, the proceeding distance in one revolution of the rotating pipe is 43.8mm . The rotational speed of the rotating pipe is 57.7rpm , and thus the maximum proceeding speed is 42.13mm/s .

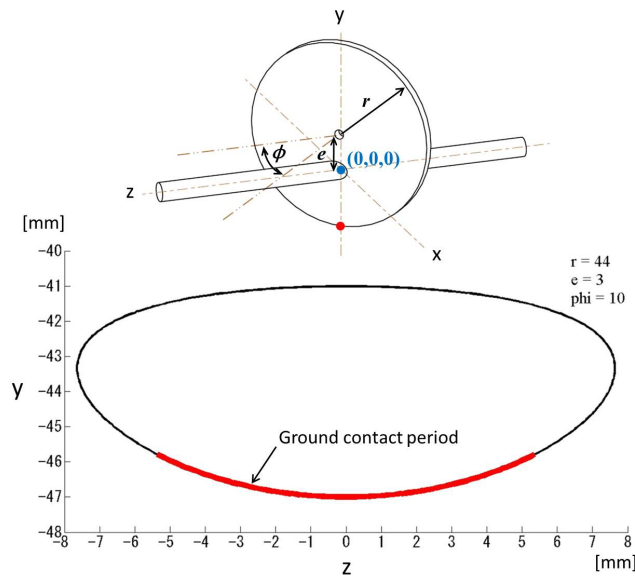
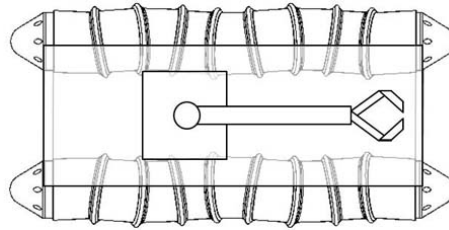
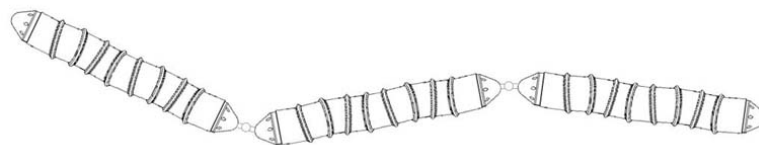


Fig. 5.1.4: Trajectory of propulsive motion

Several RS-Wave units can be connected together in different patterns for different application purposes. For example, they can be series connected to form a snake-like robot that can inspect narrow spaces; they can be parallel connected as a mobile robot to carry other operation devices. Moreover, if we remove the bellows and let the external rings rotate freely, the mechanism can propel in axial direction and rotate freely in lateral direction. Then, they can be connected as a polygon, such as triangle or square, and it becomes an omni-directional vehicle. Images of above mentioned connection patterns are shown in Fig. 5.1.5.



Parallel Connection



Series Connection

Fig. 5.1.5: Patterns of RS-Wave units connection

5.2 Mechanical Design

The RS-Wave vehicle was composed of two RS-Wave Units that were parallel connected. Fig. 5.2.1 shows the appearance of RS-Wave vehicle. The two RS-Wave units are mirror-symmetric. The previous prototype had the problem that it proceeded in deflected direction. Hence we designed this mobile robot with a parallel structure. In this case, the cancellation of lateral propulsive forces allows the robot to move straight forward along the axial direction. The specification of this model is shown in Table 5.2.1.

Table 5.2.1: Specifications of the RS-Wave Vehicle

Dimensions	$592.5mm \times 243mm \times 88mm$
Weight	$6.8kg$
Actuator	Brushless DC90W, Gear ratio $104 : 1 \times 2$
Planetary Gear Set	$2.7 : 1$
Rotation Speed	$57.7rpm$
Proceeding Speed	$42.13mm/s$



Fig. 5.2.1: Appearance of RS-Wave vehicle

5.3 Motion Control

The control diagram of RS-Wave vehicle is shown in Fig. 5.3.1. The micro controller and motor driver used in this robot are TITechSH2 Tiny Controller and 1BLDC Power Module (HiBot). To drive the robot, the signals of the rotation velocity can be input through the joystick in Fig. 5.3.2, and they are transmitted to the motors in the left and right sides respectively. The hall sensors on the motors can measure the actual rotational speed of the motor and give feedback to the micro controller. As we are concerning to make the robot as light weight and small as possible, there is no embedded battery in this robot, and the power is supplied through a tether

system.

As for the moving direction of the robot, it is simply controlled by changing the rotating direction of both motors. Since the two RS-Wave units are mirror-symmetric, when the two motors rotate in opposite direction, the robot moves forward or backward; when they rotate in the same direction, the robot turns.

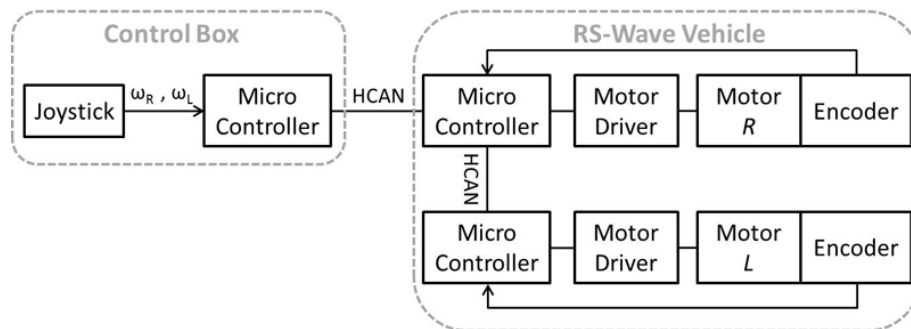


Fig. 5.3.1: Control circuit of RS-Wave Vehicle



Fig. 5.3.2: Control box of RS-Wave Vehicle

5.4 Experiment and Result

The mobility of this RS-Wave vehicle is evaluated experimentally. First, the basic motions including moving forward, moving backward, making turns were confirmed.

RS-Wave vehicle is able to make a pivot turn by propelling left and right unit in opposite direction. Figure 5.4.1 shows the robot making a left rotation for 180 degrees.

Motion experiments in several different conditions were conducted. The followings are the explanation of the experiments.

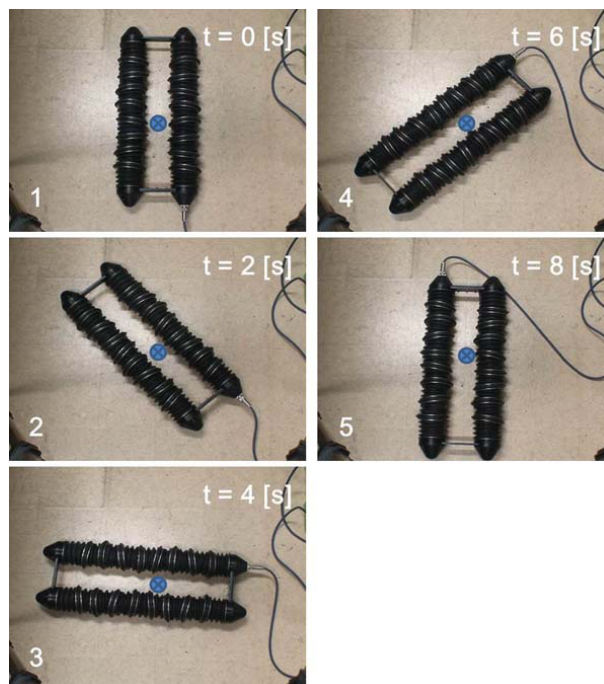


Fig. 5.4.1: Pivot turning of RS-Wave vehicle

5.4.1 Underwater

To test the water tightness of RS-Wave vehicle, it was put into a water tank. Fig. 5.4.2 shows the mobile robot moving in the water. It stayed in the water for 1 hour and it could perform proceeding and turns without any leakage. This experiment proved that RS-Wave vehicle is waterproof, and that it is able to operate underwater as well.

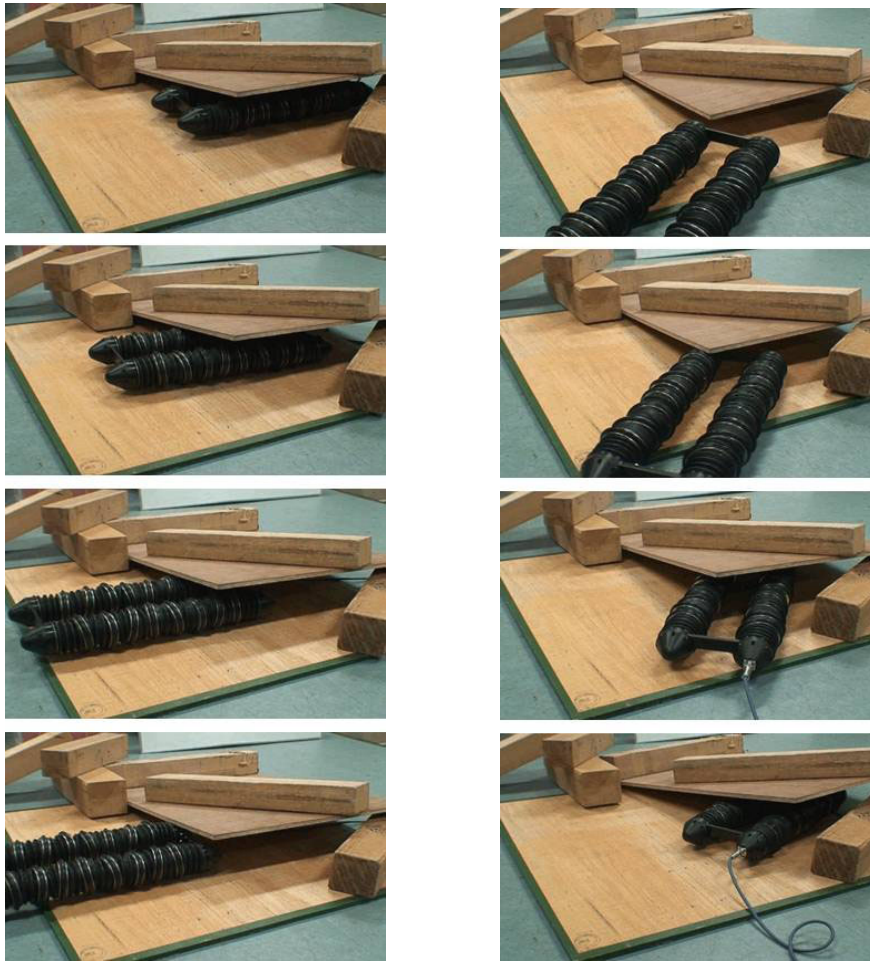


Fig. 5.4.2: Underwater experiment

5.4.2 Narrow Space

In this experiment, RS-Wave vehicle was put in a narrow space between boards. Since RS-Wave mechanism produces same direction propulsive forces from the whole contacting surface, the mobile robot can squeeze through the narrow space easily. Fig. 5.4.3(a) is the image when the mobile robot escaped from the narrow interval, and Fig. 5.4.3(b) shows the image that it squeezed into the interval.

In a further experiment, RS-Wave vehicle was put under an acrylic sheet, and weights were put on the top of the acrylic sheet as shown in Fig. 5.4.4. By giving the same input angular velocity, the proceeding speed and average current were recorded. Fig. 5.4.5 shows the result of the experiment. It reveals that even when the load is increased to $31.5kg$, the robot can still propel in the same speed and required current did not increase significantly. From this result, we expect that when RS-Wave vehicle can move in rubble and can be pressed heavily by obstacles from the top, escaping and continuing the locomotion easily.



(a) Escaping

(b) Entering

Fig. 5.4.3: Narrow space

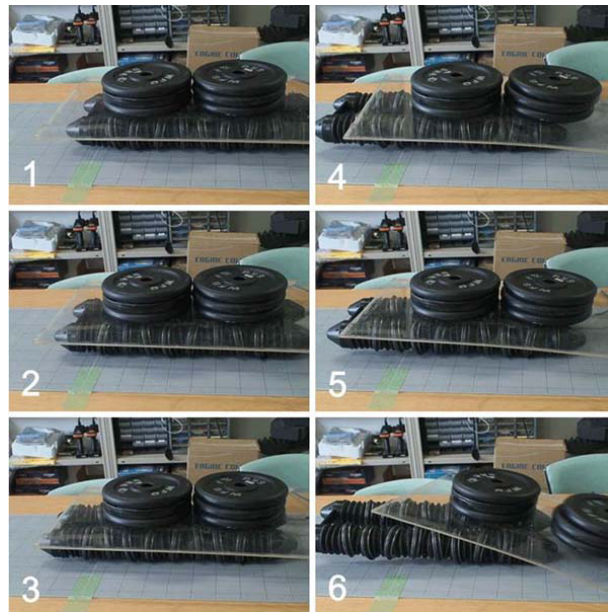


Fig. 5.4.4: Propulsion under 31.5kg load

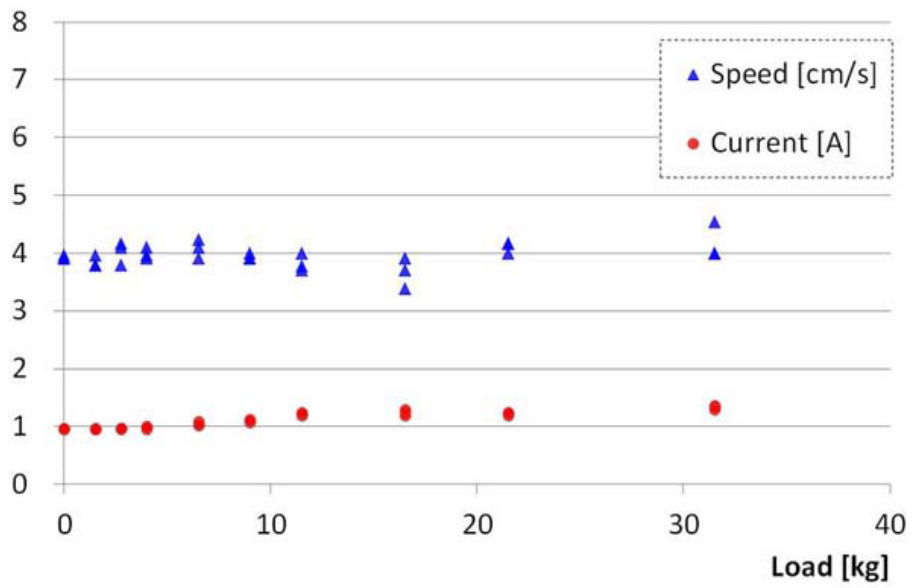


Fig. 5.4.5: Speed and current under load

5.4.3 Slope

The purpose of this experiment is to check the ability on climbing up a slope. The angle of the slope was varied from small to large. Fig. 5.4.6 is the image of the robot climbing up the slope. The final result shows that RS-Wave vehicle can climb up slopes under 15 degree angles. Due to its rigid body, the robot has difficulties climbing up a steep slope. When the robot comes to the transition area from level ground to the slope as Fig. 5.4.6(2), the middle part of its body does not contact with the ground and thus only the front and the rear parts are propelling. This makes it difficult to overcome steeper slope.

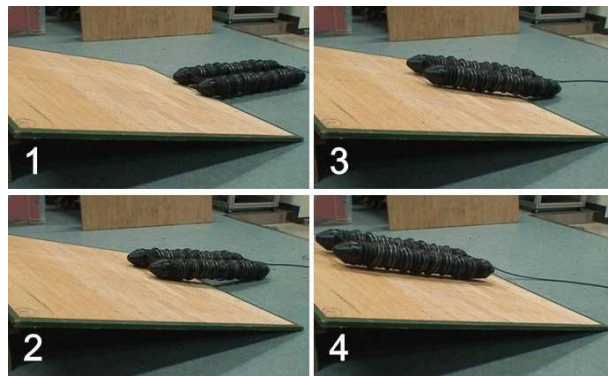


Fig. 5.4.6: Slope climbing experiment

5.4.4 Step

In the above experiments, RS-Wave vehicle were only tested on even ground. However, in real environment, there are many rough terrains. Therefore, in this experiment, we examined the mobility of the robot when facing steps. Since the eccentric inclined discs only lift up $6mm$ during propulsion, the height of the step is quite limited. The experiment result shows the maximum step this robot can overcome is about $25mm$. Fig. 5.4.7 shows the environment of the experiments.

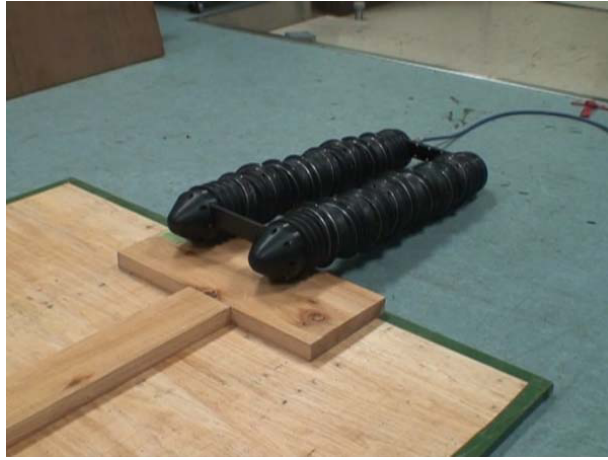


Fig. 5.4.7: Step climbing experiment

5.4.5 Soft Ground

This experiment examined RS-wave vehicle's performance on soft ground. As shown in Fig. 5.4.8, two different experiments was conducted. One is tested on a sponge, and the other is tested on the grass outdoor. In both experiment, the velocity of the robot was much slower than when it moved on solid ground. In the case of sponge, the proceeding velocity was 5.9mm/s , it was only about 14% of the normal speed on solid ground. The low speed might be caused by the retuning phase of the motion of discs. As explained in the principle of RS-Wave mechanism, the propulsive motion is generated by the eccentric inclined discs which generate circular trajectories. The bottom of the disc contact to the ground and propel the robot, then lift up and return. However, as illustrated in Fig. 5.4.9, on a soft surface the returning phase of the discs may also contact to the ground, and that causes resistance to the robot.



(a) Sponge



(b) Grass

Fig. 5.4.8: Motion on soft ground

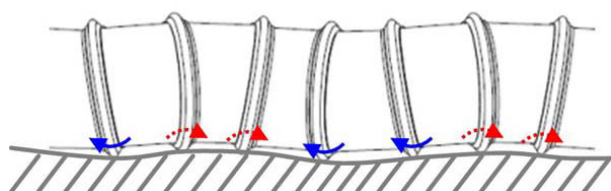


Fig. 5.4.9: Interference of returning phase

5.4.6 Flipped Over

One of the most important feature of RS-Wave mechanism is its whole body propulsion motion. This feature is not only useful when the vehicle moving in very narrow interval, but also useful when the vehicle tumbled over. For other propulsion mechanism which has single propulsive surface, the vehicle get stuck if it is upside done.

Some of the crawler vehicles may keep moving by using the upper side of the crawler, but they have to drive the crawler in opposite direction to keep moving forward. The whole surface of RS-Wave mechanism generates propulsive motion to the same direction, thus even when the robot is flipped over it could continue locomotion without changing driving direction. This feature was also examined experimentally. In the experiment, the robot fell down from a step and turned upside down, but still keep moving forward without any additional control command.

5.4.7 Summary of Experimental Result

The above experiments present the mobility of RS-Wave vehicle. It has good performance on even ground or narrow space, and also the watertight structure allows it to operate in the water as well. As for locomotion in uneven terrain, the present design is not sufficient. To improve the design, perhaps by connecting several units of this robot with lifting mechanism in between, they can overcome larger obstacles. Additionally, if the robot has an elastic shaft, it may have better terrain adaptability.

5.5 Energy Efficiency of RS-Wave Vehicle

5.5.1 Introduction of Specific Resistance

Specific resistance ε was first proposed by Gabrielli and Von in 1950[30]. It is a dimensionless quantity which is widely used for evaluating the power efficiency of locomotion. Specific resistance is defined as:

$$\varepsilon = \frac{E}{mg \cdot L} \quad (5.5.1)$$

where E is the required energy for locomotion; m is the mass of the vehicle; g is gravitational acceleration, and L is the travelling distance during the locomotion.

The E and L can be substituted by E and L by differentiating.

$$\varepsilon = \frac{dE/dt}{mg \cdot dL/dt} = \frac{P}{mg \cdot V} \quad (5.5.2)$$

The smaller value of specific resistance indicates higher energy efficiency. Many researchers had used specific resistance to evaluate the energy efficiency of their robots[31–36].

To evaluate the efficiency of RS-Wave vehicle, its specific resistance was measured.

5.5.2 Experiment on RS-Wave Vehicle

To calculate the specific resistance of RS-Wave mobile robot, at the beginning, the consumed power was measured. In order to distinguish the power consumed by the electrical device, the mechanical parts and locomotion, The power measurement was done in three different conditions as shown in Fig. 5.5.1.

First, the RS-Wave vehicle was propped up and the propelling parts do not contact to the ground. The power consumed by the electrical device P_0 was measured when 24 volt electricity was supplied but the motors were not moving. Then, the RS-Wave vehicle still stayed on the prop, but the motors were driven. The consumed power P_{NL} when there was no external load was measured. Finally, the RS-Wave vehicle was put on a flat ground and did locomotion. The consumed power P_L during locomotion was measured.

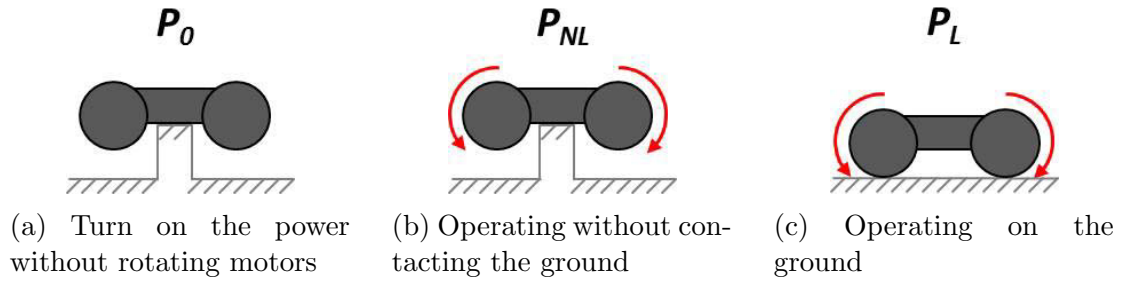


Fig. 5.5.1: Three types of power measurement

From the experimental result, P_0 was $4.19W$, and P_{NL} and P_L at maximum velocity was $21.11W$ and $21.33W$ respectively. By subtracting P_{NL} from P_L , the net power P_{net} used for locomotion can be obtained.

$$P_{net} = P_L - P_{NL} \tag{5.5.3}$$

Besides the power, the proceeding velocity of RS-Wave vehicle under different supplied voltage were also measured. The whole experiment were conducted on an smooth and even surface.

The power used for specific resistance was not clearly defined. In this experiment, two types of specific resistance were calculated; One was calculated with the total consumed power P_L during the locomotion, and the other is calculated with the net power P_{net} used for locomotion. The results are shown in Fig. 5.5.2 and Fig. 5.5.3 respectively.

In both figures, the value of specific resistance decrease as velocity increase. The specific resistance derived with P_{net} was about 0.08 to 0.15. For reference, Fig. 5.5.4 is a chart made by Gregorio, Ahmadi, and Buehler, and the curved of RS-Wave vehicle was added. In the figure, cars, human, and some mobile robots were plotted. The curves that are closer to lower-right corner have higher efficiency. Comparing

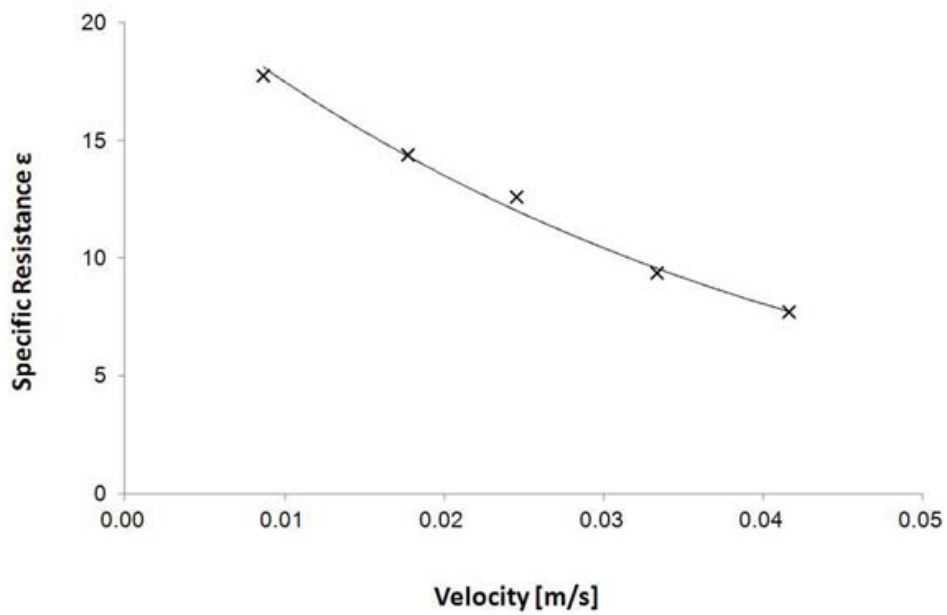


Fig. 5.5.2: Specific resistance ϵ calculated with P_L

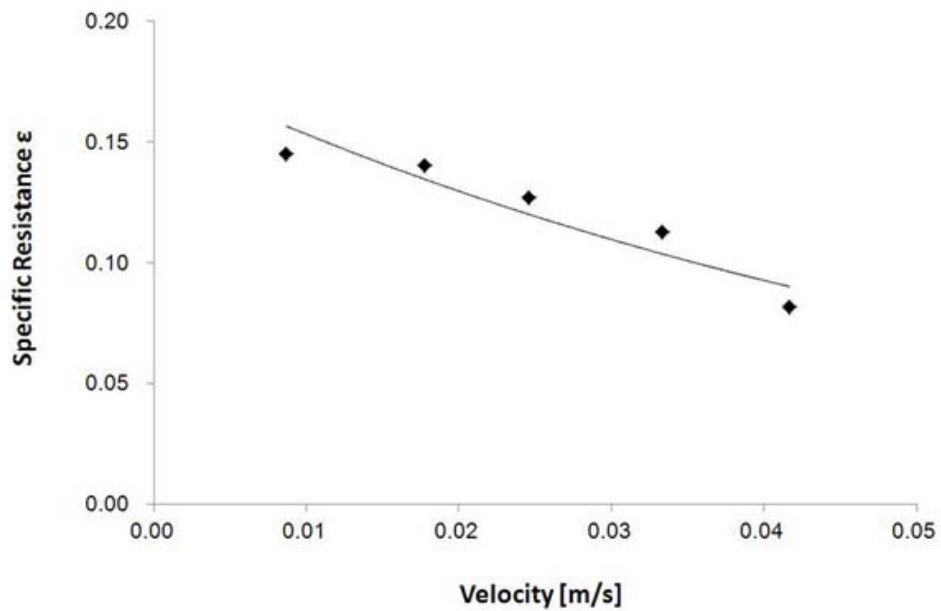


Fig. 5.5.3: Specific resistance ϵ calculated with P_{net}

with these vehicles, the efficiency of RS-Wave vehicle was relatively low. It may be owing to the high internal energy lost caused by the bellows.

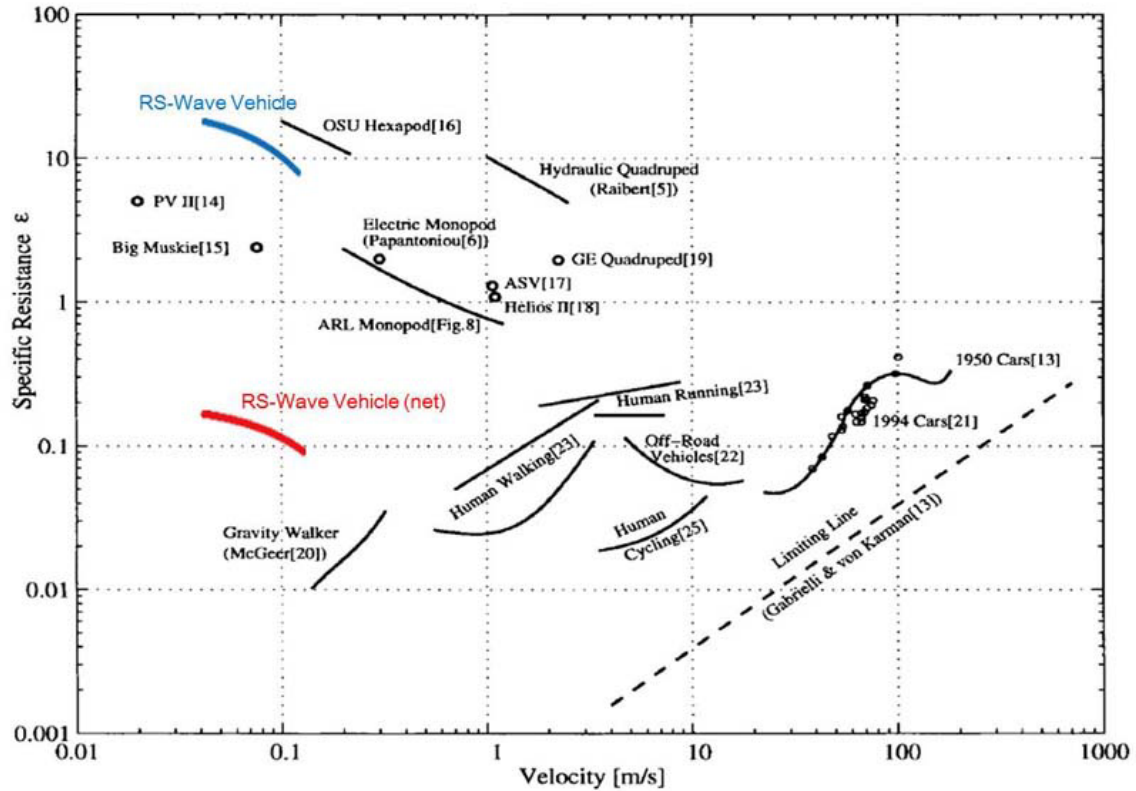


Fig. 5.5.4: Specific resistance of other vehicles

5.5.3 Energy Loss of Bellows

The resistance of bellows caused energy loss on RS-Wave vehicle. To calculate the amount of lost energy, RS-Wave vehicle without covering by bellows was also tested. Fig. 5.5.5 shows the picture of RS-Wave vehicle without bellows. The power consumptions during locomotion were measured before and after taking off the bellows. Under same environment condition, the power consumptions during locomotion of RS-Wave vehicle with bellows and without bellows were about 25.4W and 17.5W respectively. It revealed that the resistance of the bellows caused 7.9W power loss. However, without bellows, the external rings freely rotate and the vehicle

slid to sideway easily. In addition, the bearings and rotating pipe exposed and the vehicle was not waterproof. Therefore, even though the bellows cause large energy loss, they are still indispensable in this design. If we decrease the phase shift between adjacent eccentric inclined discs, the deformation of bellows may be decreased and thus the energy loss may also be reduced. But at the meanwhile, the wave length of surface wave will increase and there will be fewer contact points.



Fig. 5.5.5: RS-Wave vehicle without bellows

5.6 Chapter Summary

At the beginning of this chapter, a more compact design of RS-Wave mechanism that has build-in actuator was introduced. Then, the first mobile robot that utilize RS-Wave mechanism was presented. The vehicle was evaluated in several different environments. The vehicle was good at squeezing through narrow space, and it had good water-tightness. However, present RS-Wave vehicle was not good at soft or rough terrain, further improvement is needed. In the last part of this chapter, the efficiency of RS-Wave vehicle was evaluated by using specific resistance. The results show that its efficiency was not very ideal.

Chapter 6

Load-sensitive RS-Wave Mechanism

6.1 Introduction of Load-sensitive Mechanism

The load that apply to the robot are highly variable depending on the working condition. Take leg robots for example, the legs step on the ground and lift up over and over again for locomotion. In the case when the leg is contacting the ground, the actuator must generate a large force to support the weight of the robot. When the leg is lifted, it no longer needs to support the weight and is possible to move faster with the same power. Another example is robot arm. It is desired to have large output force when the load is heavy, and fast motion when the load is light. The robots are usually designed with high reduction ratio in order to generate sufficient force, but the output speed is then limited. To give consideration to both large output force and high speed, the actuator needs operate under a wide range from low speed to high speed. However, the most efficient operating rpm for a motor is fixed.

To make robot operate under different conditions with high energy efficiency,

variable-ratio transmission is very important. However, normal CVTs(Continuously Variable Transmission) are usually bulky and not easy to introduce in the mobile robots which need the compact shape and lightweight mechanism. In the former study of the laboratory, trial was already made to introduce commercially available traction-drive-type CVT in the robot. But it is bulky and heavy (as the mechanism depends on the large traction force and the force is made balanced with the strong structure) [37]. In the former work of the laboratory, there were some other challenges to make compact load sensitive transmission for robotic mechanisms. For example, two stage type [38, 39], traction drive type [40] and linear motion type [41]. But it is not yet commercialized a compact and lightweight load sensitive transmission.

When we think of the principle of the RS-Wave mechanism, we can find very interesting feature, that is, the function to generate the load sensitive transmission only by adding joint and spring in the discs. Increase of the mass and the size is surprisingly small. Therefore the feasibility of this function was studied, and an experiment model was made and evaluated.

6.2 RS-Wave Mechanism With Load-sensitive Mechanism

There is a trade off between output thrusting force and proceeding speed. The following equation 6.2.1 expresses the theoretical relation of input power, torque, thrusting force, and speed.

$$P = T \cdot \omega = F_t \cdot v \quad (6.2.1)$$

When the proceeding speed of RS-Wave mechanism is high, the thrusting force is relatively small; On the contrary, when RS-Wave mechanism generate larger thrusting force, the proceeding speed is slow.

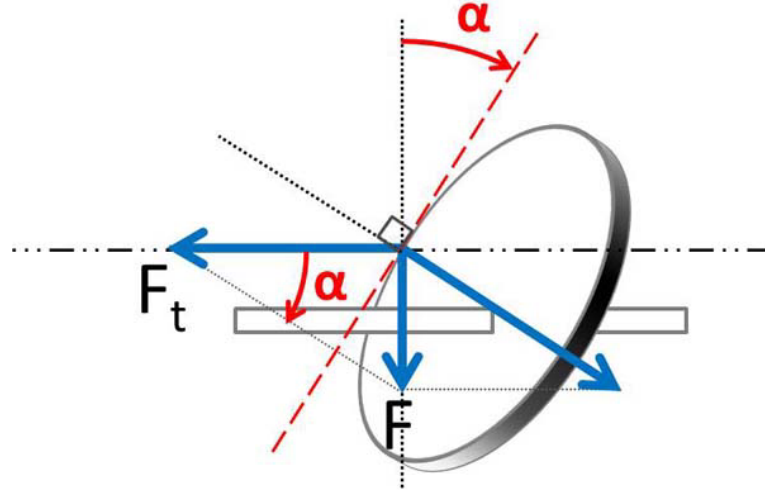


Fig. 6.2.1: Thrusting force of RS-Wave mechanism (Top view)

Regarding to RS-Wave mechanism, the thrusting force in axial direction is related to the inclination of the rotating disc. More precisely speaking, it is related to the angle of the disc's tangent line at the contact point as shown in Fig. 6.2.1. Angle α is defined as the include angle of the disc's tangent line and lateral direction of the mechanism. Assume T is output torque of the rotating shaft, and F_t is the thrusting force in axial direction. Then, the relation of these parameters can be written as:

$$F = \frac{T}{r_c} \quad (6.2.2)$$

$$F_t = F \cos \alpha \quad (6.2.3)$$

where F is the output force at the contact point, and r_c is the radius from the ro-

tating axis to the contact point. Therefore, when the motor of RS-Wave mechanism output constant torque, if the contact angle α is large, the thrusting force becomes small; On the other hand, when the contact angle α is smaller, the thrusting force becomes larger.

The contact angle α varies with the rotational angle of the disc. Fig. 6.2.2 shows the variation of α during one revolution of the disc. The minimum angle and maximum angle are $-\phi$ and ϕ respectively, and ϕ is the inclination of the eccentric inclined disc. Also, at any rotational angle, disc with smaller ϕ has smaller contact angle α . Consequently, by changing the inclination ϕ , contact angle α can be varied, and then the thrusting force F_t may also be changed.

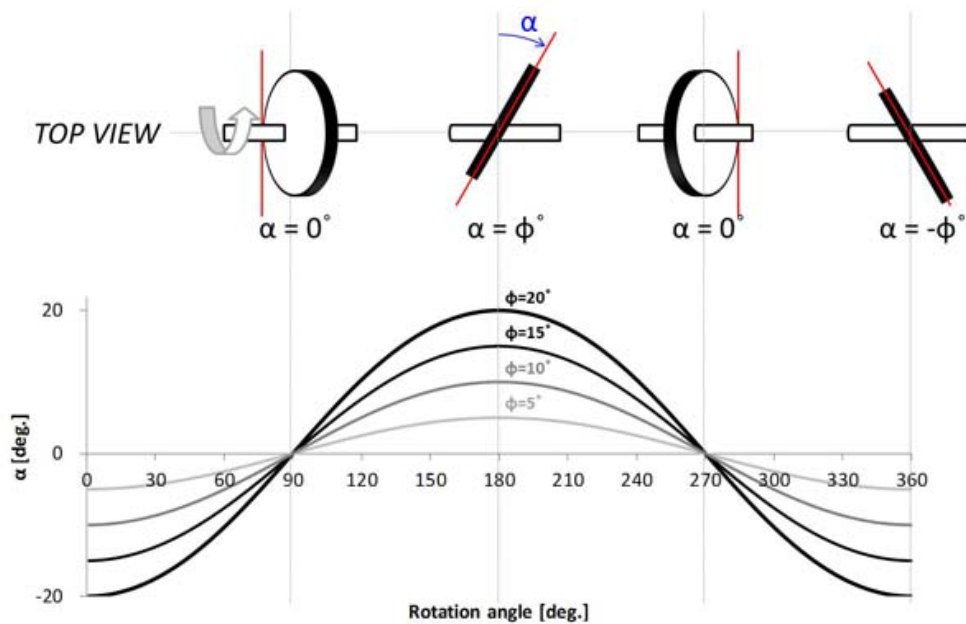


Fig. 6.2.2: Tangent angle at contact point

Regarding to the relations between thrusting force and inclination of the disc, the idea of applying load-sensitive mechanism on RS-Wave mechanism was proposed. Instead of the discs with fixed inclination, the inclination of the discs on load-sensitive RS-Wave mechanism are variable in certain range. With this mechanism,

when the mobile robot is on an even ground where it can move forward easily without large output force, it can use large inclination ϕ to move in maximum speed. On the other hand, if the mobile robot is climbing up on a slope, it takes larger output force to climb up. In this case, it can change to smaller ϕ and move slower but with stronger thrusting force.

Figure 6.2.3 shows the basic concept of load-sensitive RS-Wave mechanism. The disc is fixed on the rotating shaft with a pin. There is a spring keeps pulling the disc and thus cause the inclination. At normal situation, the load-sensitive RS-Wave mechanism keeps maximum inclination and moves in highest speed. When there is large force applied to the contact point on the disc, the inclination ϕ decreases and RS-Wave mechanism may generates larger thrusting force.

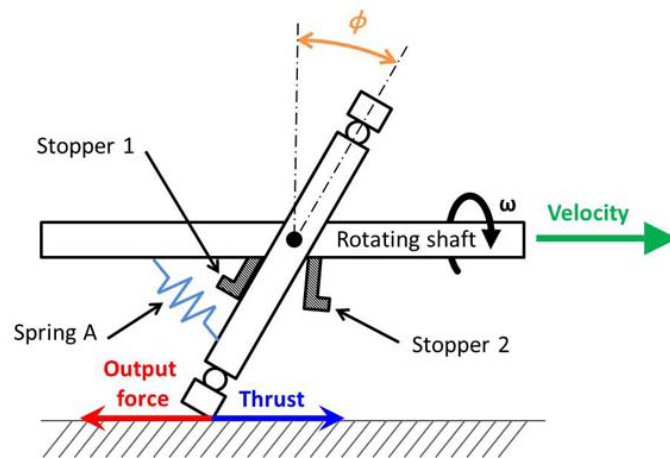


Fig. 6.2.3: Concept of load-sensitive RS-Wave mechanism

6.3 Mechanical Design

A experiment was conducted to test the feasibility of load-sensitive mechanism. Fig. 6.3.1 shows the whole experiment device. The experiment model with a single eccentric incline disc was installed, and a slider was set below the disc. The slider

was pulled by a load, which is the bottle of water in the picture. The purpose of this experiment was to verify whether a disc with load-sensitive design can pull up heavier load than the disc without load-sensitive mechanism.

Figure 6.3.2 shows a close-up view of the experiment device. A single unit of eccentric inclined disc is fix on a vertical linear guide, and below the unit is a slider pulled by certain payload. The vertical linear guide is positioned at the height that makes the disc contact to the slider for only the propelling period during each rotation cycle, so that the returning phase does not affect the experiment result. From the payload of the slider, the thrusting force of the mechanism can be known. As for the proceeding speed, it can be calculated from the displacement and time.

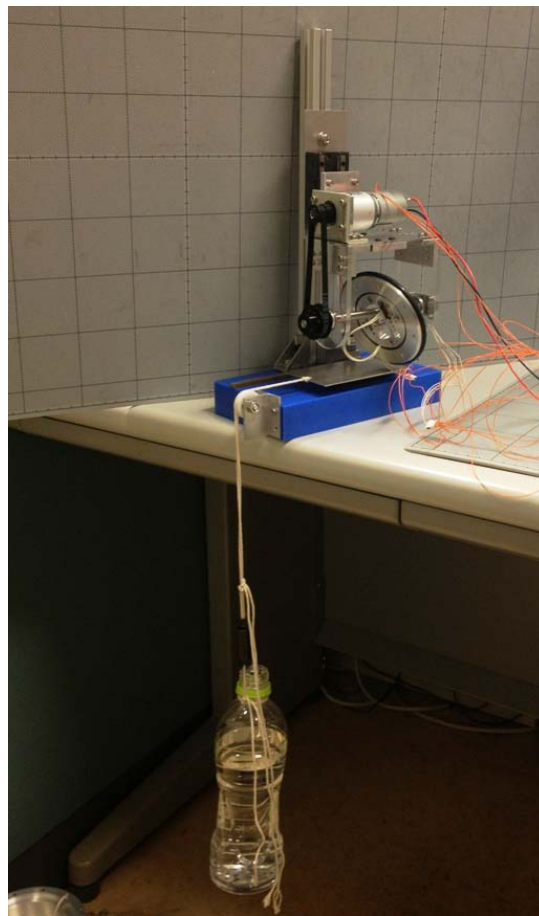


Fig. 6.3.1: Experiment device for load-sensitive RS-Wave mechanism

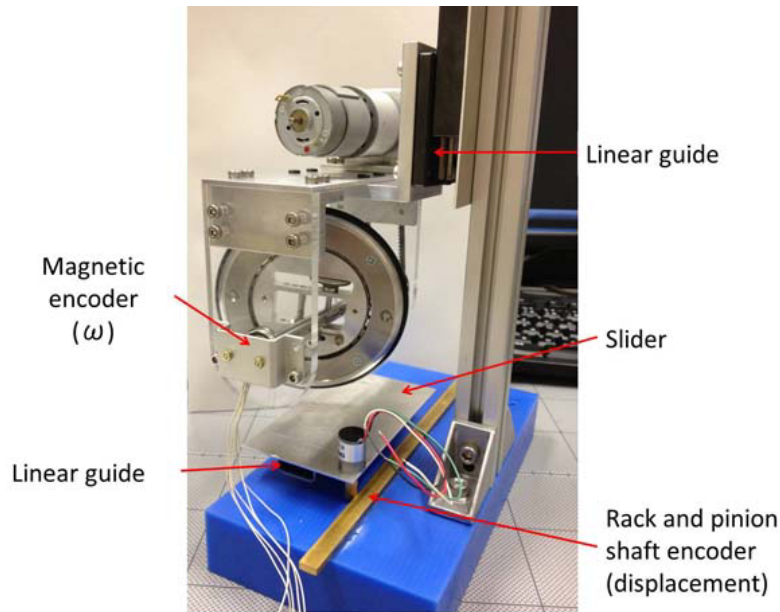


Fig. 6.3.2: Experiment installation

The design of the eccentric inclined disc was changed in order to install load-sensitive mechanism. Fig. 6.3.3 shows the detail design of the disc. The disc is composed of two discs clamped together (disc A and B). There are two small rods in the middle, one is the axis of inclination (rod C), and the other is for holding the spring (rod D). There are six grooves on the discs, thus the eccentricity ε_x can be changed by placing rod C in a different groove. At meanwhile, the distance between the two rods is fixed so that the relative position of the spring remains the same. The diameter of the grooves are slightly larger than the diameter of the rods, so the rods can rotate freely in the grooves. A long screw is fixed on one end of rod C and passes through a slot. This slot works as a limiter that restrict the inclination ϕ in certain range. In addition, a magnet is fixed on the other end of rod C, and the angle of ϕ is measured by a magnetic encoder.

Figure 6.3.4 shows how the disc unit was fixed on the rotating shaft in two different views. There was a d-cut on rod C and thus the rod could be clamped

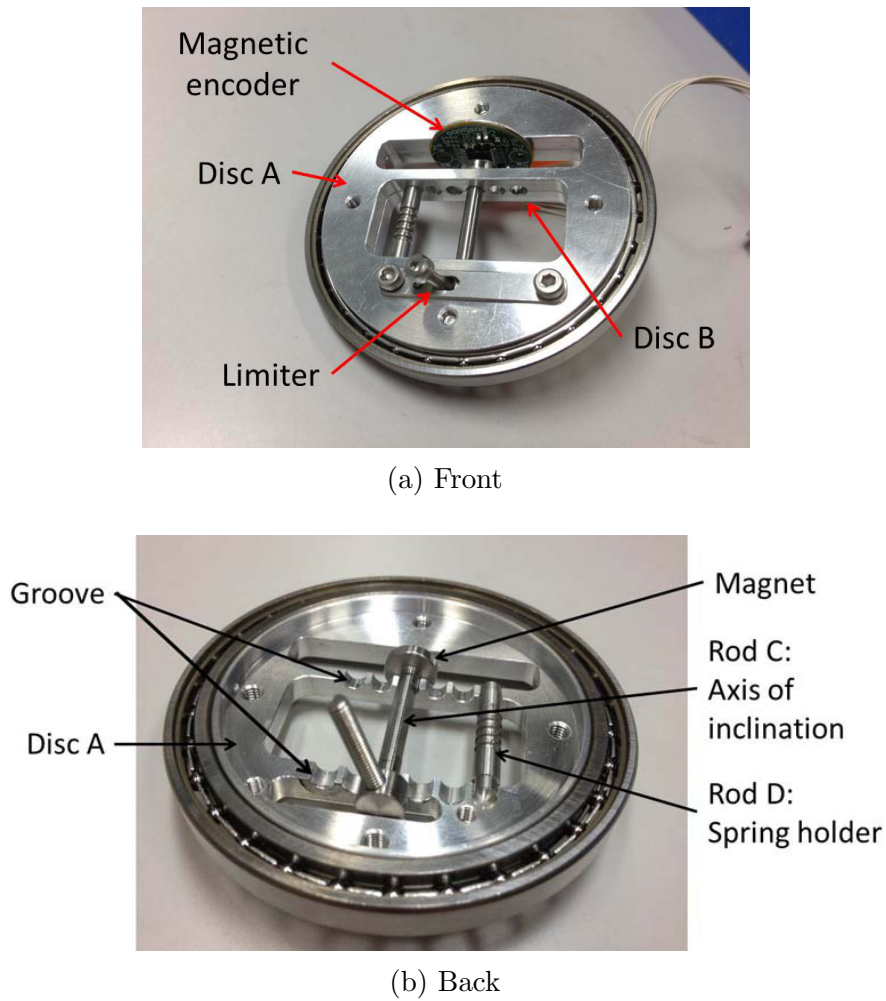
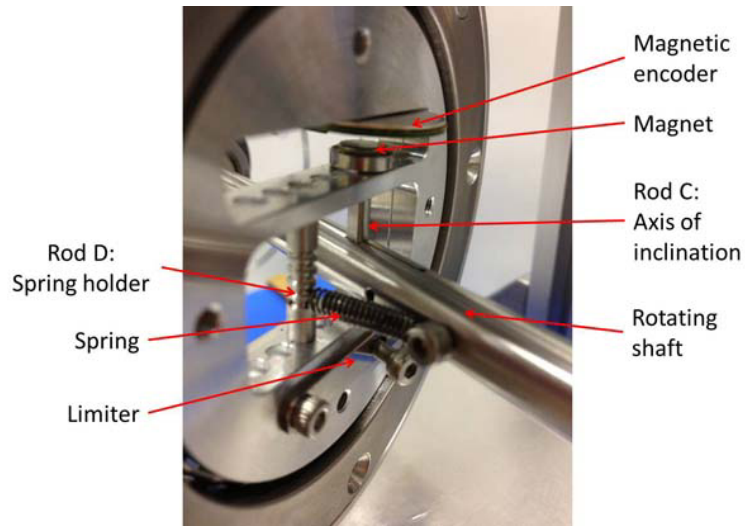
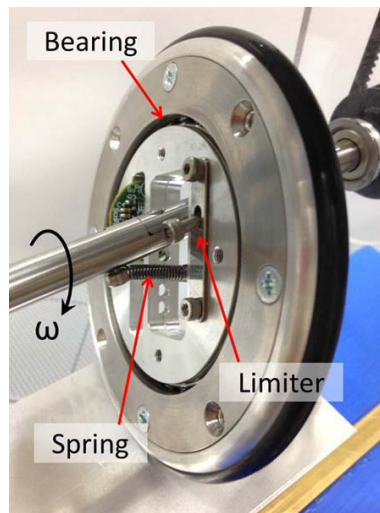


Fig. 6.3.3: Disc for load-sensitive experiment

firmly to the rotating shaft without spinning. This ensured the magnetic encoder get the correct angle. In addition, the clamping position on rod C was adjustable, which generated eccentricity in another direction(ε_y). A spring was fixed between the rotating shaft and the rod D, it kept the disc tend to incline in maximum angle. The rotational speed of the shaft ω was also measured by a magnetic encoder as shown in Fig. 6.3.2.



(a) Left



(b) Bottom

Fig. 6.3.4: Disc fixed on the rotating shaft

The previous prototype only had eccentricity along y-axis, but in that case the external load may rotate the disc in opposite direction during the ground-contacting period. Therefore, an additional eccentricity along x-axis was added in this model. Fig. 6.3.5 illustrates the difference of the ground-contacting region.

The diagram in Fig. 6.3.6 shows the electrical system of the experiment device. A micro computer was connected to four sensors and a motor controller. The four

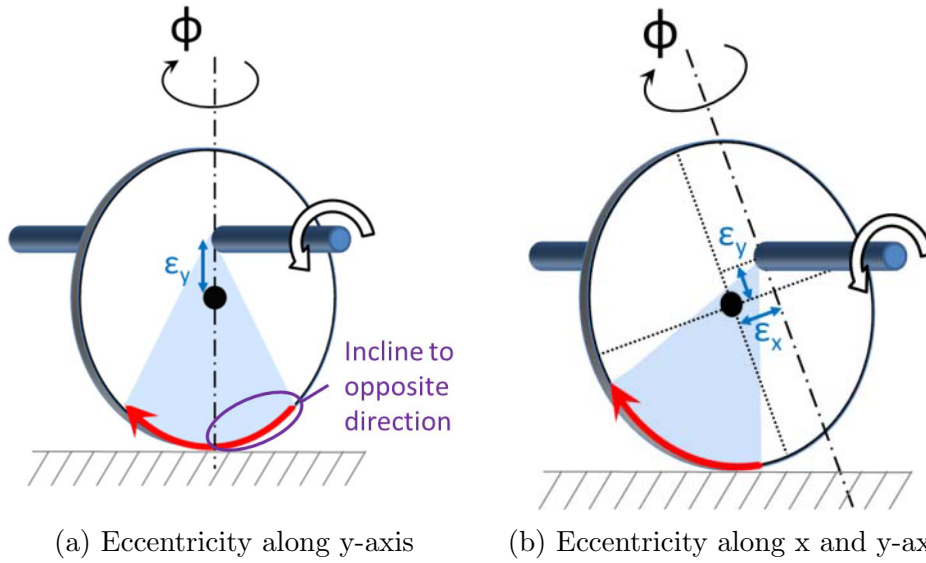


Fig. 6.3.5: Effect of the eccentricity direction to ground-contacting region

sensors measured inclination ϕ , rotational speed ω , displacement of the slider, and current of the motor respectively. The specification of the motor and each sensor are shown in Table 6.3.1.

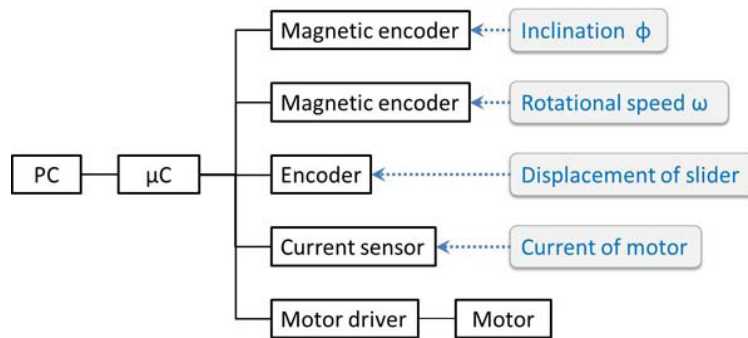


Fig. 6.3.6: Electrical system of experiment device

Table 6.3.1: Specification of electronic devices

<i>Item</i>	<i>Model</i>	<i>Specification</i>
Controller	Hibot, TITechSH2	
Motor	Mabuchi, RS-385PH	12V DC, gear ratio 1 : 100
Motor controller	Hibot, 1AxisDCPower Module	
Magnetic encoder	Sustainable Robotics, KP1013	16 bit resolution
Encoder	Copal, RE12D	300 resolution
Current sensor	ACS714	-5A to 5A, Sensitivity 185mV/A

6.4 Experiment and Result

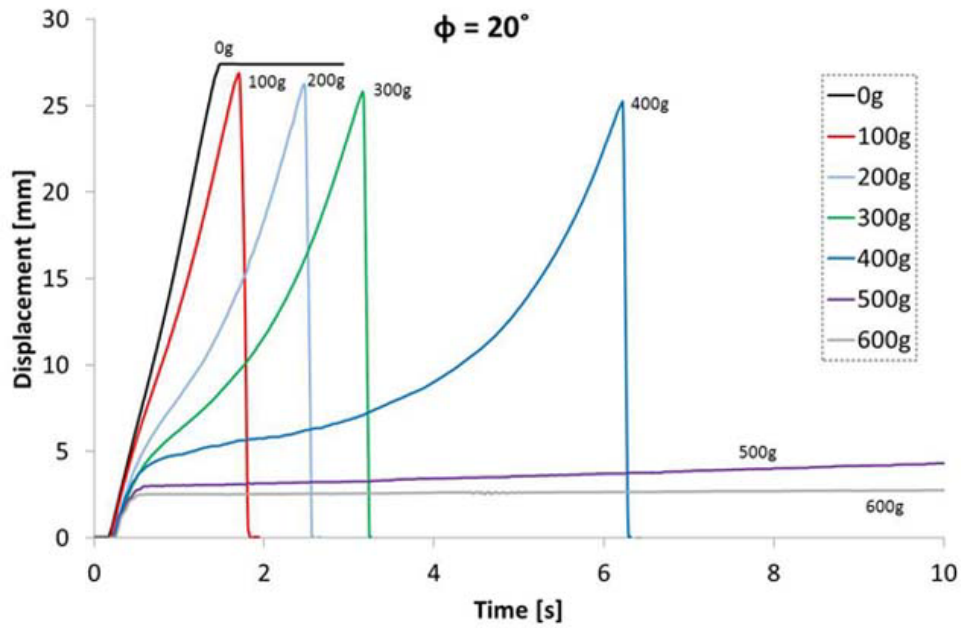
The performance of load-sensitive mechanism for RS-Wave mechanism was evaluated by experiments. First of all, before using the load-sensitive mechanism, the original discs with fixed inclination angle was used in order to verify the relation between inclination and thrusting force. Then, the experiment with load-sensitive disc was conducted. In the second experiment, a disc with fixed inclination was also used for comparison. The experiment methods and the results are explained in the following sections.

6.4.1 Propulsive motion with fixed inclination

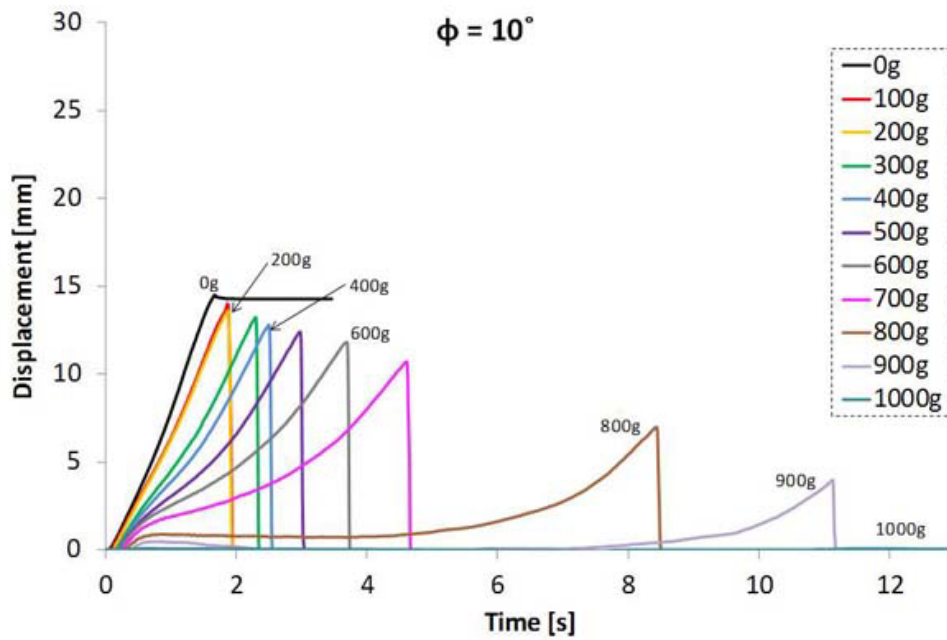
In this experiment, the adjustable disc in section 4.3.3 was installed to the new experiment device. The electric power of the experiment device was given by a DC power supply. The output current of the power supply was limited in a small value in order to output constant current and make the motor output constant torque. Discs with same eccentricity ($6mm$) but different inclination angle (20 and 10 degrees) were tested. During the experiment, the weight of the load was increased $100g$ gradually

until the mechanism could not propel any more. The displacement of the slider, the weight of load, and time were recorded.

Figure 6.3.4 shows the result of this experiment. Note that most of the curve drop down to zero at the end except for the curve of no load. It was because the slider was pulled by the load, and thus it returned to the start point immediately when the disc lifted up and separated from the slider. The chart reveals as the load increased, the time for propulsive motion also increased, which means the propelling speed decreased. The upper chart is the result of 20 degree inclination. When the load was lighter than 400g, the mechanism could be propelled over 25mm within 6.5 seconds. But from 500g, the slope of the curve dropped suddenly, the motion became really slow which is considered not practical for real application. Thus the maximum supportable load was about 400g. As for the result of 10 degree inclination, the propelling distance was around 11 to 14 mm under the load within 700g. The motion with the load over 800g was slow, and it stopped at 1kg. Comparing the two charts, it is apparent that when the inclination changed from 20 to 10 degrees, the propelling distance decreased, so the propelling speed became slower. However, the maximum supportable load increased, which means the thrusting force was stronger. This result verified the assumption that smaller inclination angle generates larger thrusting force was correct.



(a) Inclination $\phi = 20^\circ$



(b) Inclination $\phi = 10^\circ$

Fig. 6.4.1: Propelling displacement under varying payload

6.4.2 Effect of load-sensitive mechanism

In this experiment, the effect of load-sensitive RS-Wave mechanism was evaluated. The weight of the load was set to be constant at $500g$, which is equivalent to pulling by $4.9N$ force. Experiments of three different models were conducted. The experiment condition of each model is shown in Table 6.4.1. Experiment **A** and **B** used load-sensitive mechanism with different spring constant. The inclination range was limited in between 16 to 20 degree in both experiments. Experiment **C** was a control group, a disc with 20 degree inclination was used. It can also be regarded as using a spring with infinitely large spring constant.

Table 6.4.1: Experiment condition

	A	B	C
Inclination ϕ [deg.]	16 20	16 20	20(fixed)
Spring constant [N/mm]	1.77	3.43	∞

The experimental result is shown in Fig. 6.4.2. The curves on the lower part are the change of propelling displacement, the peaks of curve A, B, C were located from left to right just in order. In experiment **C**, at the moment the disc contact to the slider, the slider was pushed for about $2mm$. But after that, the rotating of the mechanism became very slow for few seconds until it finally finished the propulsive motion. It took about 11 seconds in total. In experiment **B**, the mechanism also paused for a while when it started contact to the slider, but the total time was about 7 seconds, which is shorter than model **C**. As for experiment **A**, the rotation did not pause, and it finished the propulsive motion in shortest time among the three models. The curves on the upper part of the chart indicate the change of inclination angle. As expected, the disc with load-sensitive mechanism decreased the angle

while facing large loading force. Spring of model A had smaller spring constant, thus the angle dropped to the lower limitation quickly. On the other hand, model B had stronger spring, so the inclination changed slower. In addition, owing to the spring force, the inclination returned to maximum angle when the propulsive motion finished and the discs separated from the slider.

As explained in section 6.2, the contact angle α is directly related to the thrusting force. Thus, the variation of α is also a important factor for discussion. The angle α was not measured in the experiment, but from the data of rotational angle of the shaft and inclination ϕ , the angle α can be calculated. The detailed processing program is included in Appendix C.

The experimental result with contact angle α is shown in Fig. 6.4.3. In general, at the first second in the figure, the discs were not contact to the slider yet, thus the the curve of α were consist to the theoretical curve that increase to value of maximum ϕ and about to drop down until $-\phi$. However, the smooth rotation were stopped by the loading force, and the curve of α became flat. Since the shaft were still rotating slowly, the α keep decreasing gradually. Finally, when α decreased to certain level, the mechanism had enough thrusting force and the propulsive motions speeded up. The differences between A, B, and C were clear, the load-sensitive mechanism allowed model A and B adjust their inclination to smaller ϕ . Thus the angle α became smaller than model C, and they reached sufficient thrusting force much faster. Nevertheless, the propelled distance decreased while using load-sensitive mechanism. It was the trade-off of the mechanism.

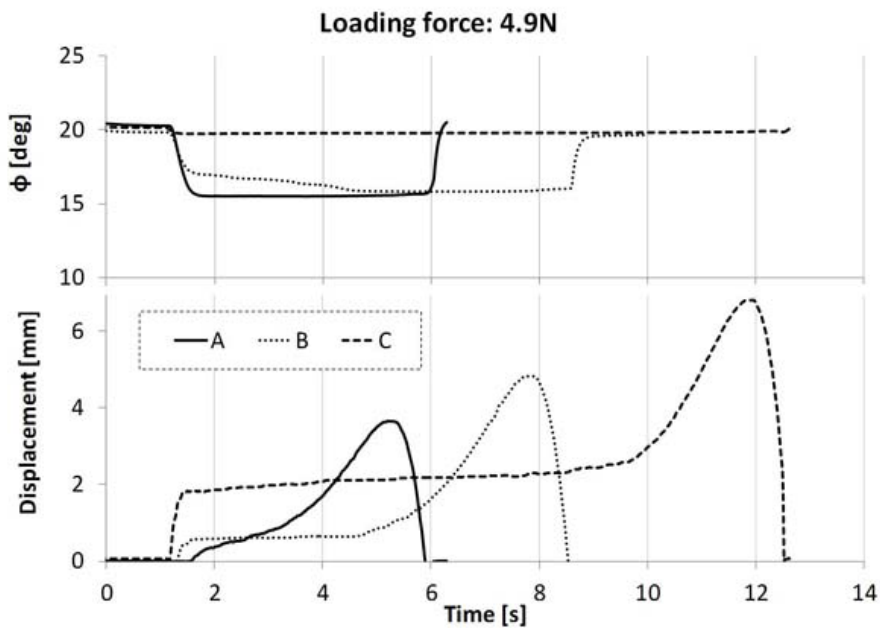


Fig. 6.4.2: Variation of inclination and propelling displacement

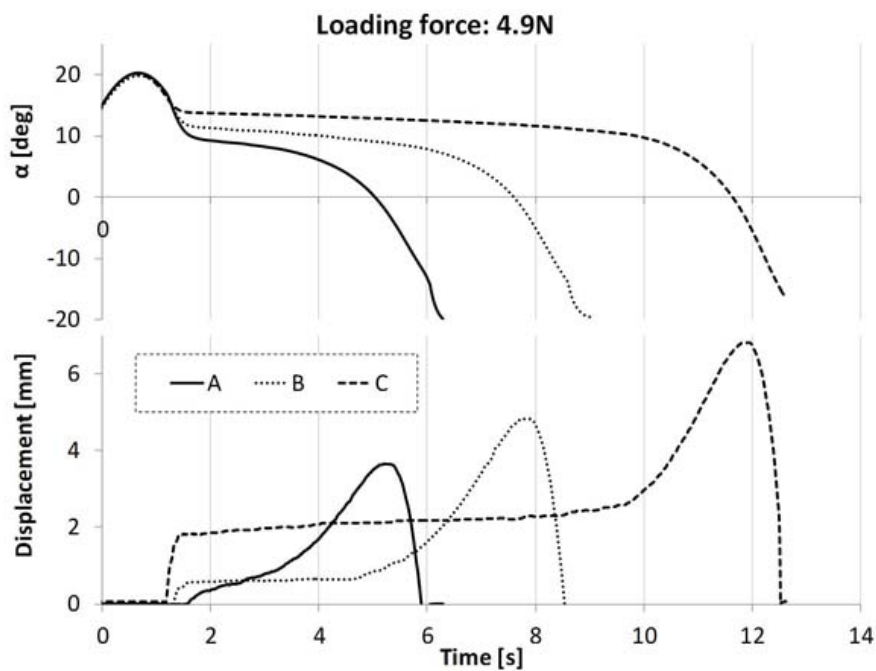


Fig. 6.4.3: Variation of contact angle and propelling displacement

6.5 Discussion

The experimental results confirmed the feasibility of load-sensitive RS-Wave mechanism. The disc with load-sensitive mechanism could keep rotation more easily when the load was heavy. To optimize the mechanism, further analysis is required. Several factors are related to the performance of the mechanism.

First, regarding to the sensitivity of the mechanism, the limitation of inclination angle and spring constant are important. As shown in the experiments, using the spring with smaller spring constant make the mechanism more sensitive, but it may results in low-speed locomotion even when the load is small. Second, the allocation of the inclination axis and the ground contacting region are also important. For example, if the contact point is on the inclination axis, the inclination does not change even if the loading force is very strong. Fig. 6.5.1 shows the image of the disc, the red arrow indicates the region of the ground contact points. In the case in the figure, when the disc starts contacting, the distance between contact point and the inclination axis is short; but when the disc keeps rotating, the distance increases, thus the same loading force may cause larger moment around the inclination axis. The contacting region is determined by the inclination ϕ , eccentricity ε_x and ε_y , and the phase shift of adjacent disc in real application. The inclination and eccentricity affect the position of contact region, and the phase shift affects the length of contact region. In the case of 90 degree phase shift, each disc contacts the ground for 90 degree in one revolution. If the phase shift is smaller, then the contact region on the disc will also be narrower.

The optimal design of these above mentioned factors are not clear yet. Therefore, further analysis of these factors will be one of the study subject in the future work.

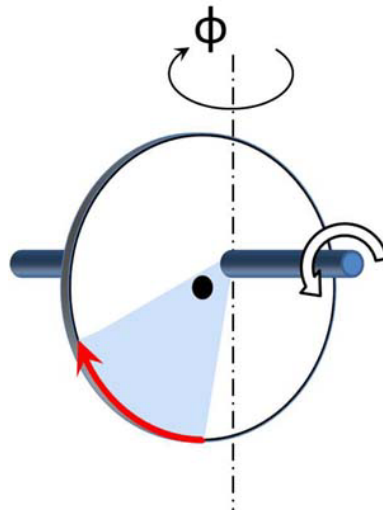


Fig. 6.5.1: Contacting region of the disc

6.6 Chapter Summary

In this chapter, the load-sensitive mechanism for RS-Wave mechanism was proposed. The purpose is to improve the efficiency of RS-Wave mechanism. With load-sensitive mechanism, the propulsion mechanism may adjust its output thrusting force and velocity according to the environment condition. An experiment device for load-sensitive RS-Wave mechanism was designed and the feasibility was verified experimentally.

Chapter 7

Conclusions and Future Work

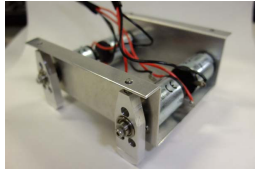


7.1 Conclusion

At the beginning of this thesis, the importance of water/dust-proof mechanism for mobile robot in hostile environment was explained, and a general view of previous studies were discussed.

In this study, we focus on developing a new propulsion mechanism with simple and water/dust-proof structure. “Surface Wave Mechanism” was proposed and it features in no exposed rotating shaft and water/dust-proof structure.

Three different prototypes of Surface Wave Mechanism were built and evaluated. Table 7.1.1 shows the comparison of the three different mechanisms. Surface Wave Mechanism PD-I generated vibration with eccentric cylinders, it was capable for reducing friction and generating propulsion. Surface Wave Mechanism PD-II utilized crankshaft for propulsion, and it proved to have good maneuverability and water-tightness. The surface wave was generated from only one surface of these two mechanisms. To improve this, Rotary Surface Wave Mechanism PL-I (RS-Wave mechanism) was proposed. It had a novel structure with two unique features: (1) *Whole surface propulsion generated by a single actuator.* (2) *No exposed infi-*

Table 7.1.1: Comparison of the three proposed Surface Wave Mechanisms

	Perpendicular type		Parallel type
	PD-I	PD-II	RS-Wave Vehicle
			
Number of motor	4	2	2
Weight	0.344 kg	0.133 kg	6.8 kg
Velocity	108.7 mm/s	58.0 mm/s	42.1 mm/s
Power consumption	0.8 W	2.4 W	21.3 W
Propulsive surface	Single (lower surface)		Whole surface
	<ul style="list-style-type: none"> • Fast, but unstable • Can be used for reducing friction of vehicles 	<ul style="list-style-type: none"> • Stable 	<ul style="list-style-type: none"> • Stable • Suitable for narrow space

nite rotating shaft. The experimental result of the prototype showed that steady and smooth propulsion was generated. The mechanical characteristics of RS-Wave mechanism were verified with the first prototype, and the design had been modified into a more compact and practical structure for future applications.

Surface Wave Mechanism still had some defects. For example, if the backstroke of the propelling part contact to the ground especially on a soft terrain, it may drag the mechanism backward and mobility will be decreased. Besides, the propulsive motion was not as efficient as wheel or crawler. Nevertheless, it has exceptional feature of water and dust free locomotion and tangle free motion against fiber-like obstacles exist in the terrain. Especially, in the case of RS-Wave mechanism, it has additional feature to generate wave motion all along the cylindrical surface of the mechanism.

A vehicle that applied RS-Wave mechanism was built and examined experimentally. Its whole body propulsive motion allows it to go through narrow space

easily. And the watertightness was also verified. But the present structure was not sufficient for rough terrain.

A load-sensitive mechanism for RS-Wave mechanism was proposed. It allows the mechanism to adjust output force and velocity according to the terrain condition. A initial experiment proved the feasibility of the load-sensitive RS-Wave mechanism.

7.2 Possible Applications of RS-Wave Mechanism

7.2.1 Inspection Robot

One of the possible applications is inspection in ceilings or under-floor area where the space is narrow and may be full with dust. Of course we need perfect watertight feature in those environment. The whole surface propelling motion and waterproof feature of RS-Wave mechanism may be suitable for this kind of environment. Fig. 7.2.1 illustrates a snake-like robot that enters underfloor area and spreads some protective agent for preventing termites.

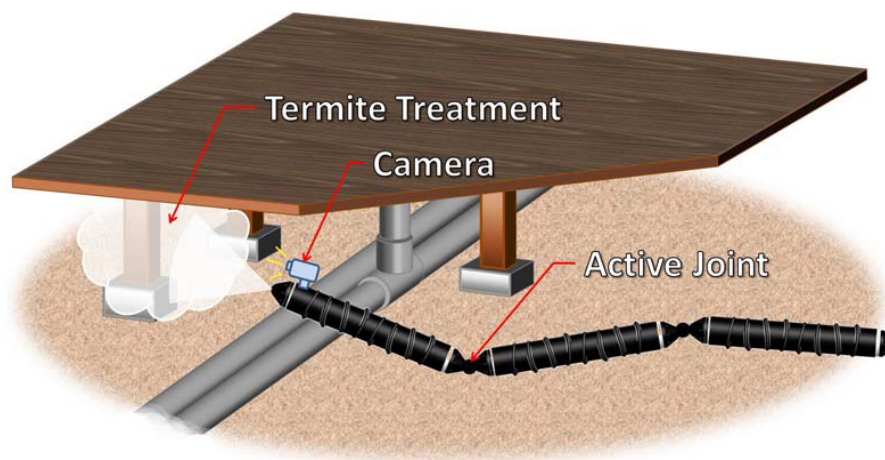


Fig. 7.2.1: Underfloor inspection robot

7.2.2 In-pipe Robot

The principle of RS-Wave mechanism may also be applied to in-pipe robot. Fig. 7.2.2 shows the image of a in-pipe robot. It consists of an elastic central shaft which is mounted with a series of eccentric inclined discs. Just as RS-Wave mechanism, the external part of the discs also have large bore bearings. The elasticity of the shaft and the eccentricity of the disc could ensure enough supporting force in lateral direction.

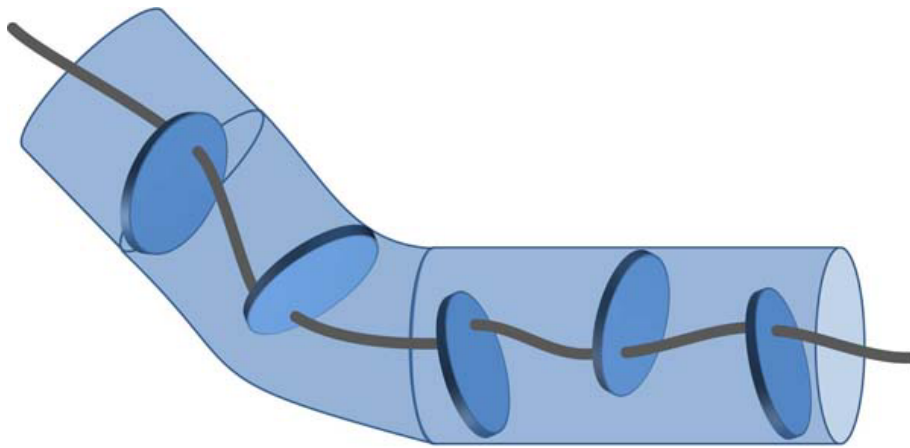


Fig. 7.2.2: In-pipe robot using RS-Wave mechanism

7.3 Future Work

There are some issues that need further studies in the future:

First, the present model of RS-Wave mechanism is not sufficient in locomotion in rough terrain. Therefore, to improve its terrain adaptation ability is an important issue for the future research. The possible solution might be connecting multi-unit RS-Wave mechanism and add active bending joints between the RS-Wave units. In addition, using an elastic rotating shaft instead of the rigid one might be another possible solution.

Second, we have verified the feasibility of load-sensitive mechanism for RS-Wave mechanism, the optimal design parameters is not clear yet. Therefore, further analysis is needed on the related factors such as allocation of spring axis, phase shift between discs, spring constant, and the inclination limitation of the discs. Besides, another future work is studying on the synchronization of disc inclination. The disc in present experiment device always returned to maximum inclination after the contact region. The potential energy stored in the spring was released and wasted. If the inclination change could be transmitted to other discs as shown in Fig. 7.3.1, then the next disc could also bend to ideal inclination before contacting to the ground, the efficiency of the mechanism could be higher.

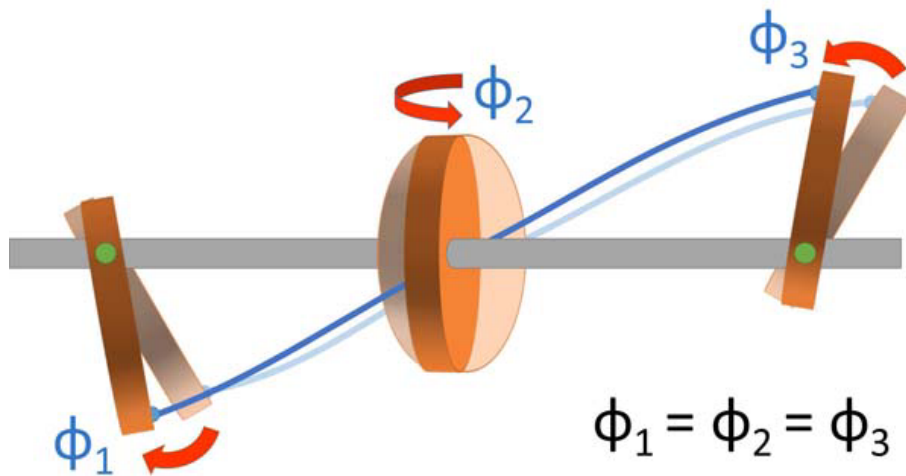


Fig. 7.3.1: Synchronized load-sensitive RS-Wave mechanism

Finally, since RS-Wave mechanism is a unique and new propulsion mechanism, there might be some suitable applications that are not developed yet. Thus, one important future work is seeking for other possible application for RS-Wave mechanism.

7.4 Chapter Summary

In the final chapter of this thesis, the review of the whole study was summarized. Some of the possible application of RS-Wave mechanism was illustrated at the end. Finally, the topics remained for further research were discussed.

Bibliography

- [1] “Annual economic financial report,” 2013. [Online]. Available: <http://www5.cao.go.jp/j-j/wp/wp-je13/index.html>
- [2] G. Granosik, “Hypermobile robots,” *New Approaches in Automation and Robotics*, pp. 315–332, 2008.
- [3] K. Isaki, A. Niitsuma, M. Konyo, F. Takemura, and S. Tadokoro, “Development of an active flexible cable by ciliary vibration drive for scope camera,” in *2006 IEEE/RSJ International Conference on Intelligent Robots and Systems*. IEEE, 2006, pp. 3946–3951.
- [4] K. Hatazaki, M. Konyo, K. Isaki, S. Tadokoro, and F. Takemura, “Active scope camera for urban search and rescue,” in *2007 IEEE/RSJ International Conference on Intelligent Robots and Systems (IROS)*. IEEE, 2007, pp. 2596–2602.
- [5] H. Ohno and S. Hirose, “Design of slim slime robot and its gait of locomotion,” in *2001 IEEE/RSJ International Conference on Intelligent Robots and Systems*, vol. 2. IEEE, 2001, pp. 707–715.
- [6] H. Omori, T. Hayakawa, and T. Nakamura, “Locomotion and turning patterns of a peristaltic crawling earthworm robot composed of flexible units,” in *2008 IEEE/RSJ International Conference on Intelligent Robots and Systems (IROS)*. IEEE, 2008, pp. 1630–1635.

- [7] M. Ono and S. Kato, “A study of an earthworm type inspection robot movable in long pipes,” *International Journal of Advanced Robotic Systems*, vol. 7, no. 1, pp. 085–090, 2010.
- [8] A. M. Bertetto and M. Ruggiu, “In-pipe inch-worm pneumatic flexible robot,” in *2001 IEEE/ASME International Conference on Advanced Intelligent Mechatronics*, vol. 2. IEEE, 2001, pp. 1226–1231.
- [9] A. S. Boxerbaum, H. J. Chiel, and R. D. Quinn, “A new theory and methods for creating peristaltic motion in a robotic platform,” in *2010 IEEE International Conference on Robotics and Automation (ICRA)*. IEEE, 2010, pp. 1221–1227.
- [10] S. Kim, E. Hawkes, K. Cho, M. Joldaz, J. Foley, and R. Wood, “Micro artificial muscle fiber using niti spring for soft robotics,” in *2009 IEEE/RSJ International Conference on Intelligent Robots and Systems (IROS)*, 2009, pp. 2228–2234.
- [11] J. C. McKenna, D. J. Anhalt, F. M. Bronson, H. B. Brown, M. Schwerin, E. Shamma, and H. Choset, “Toroidal skin drive for snake robot locomotion,” in *2008 IEEE International Conference on Robotics and Automation (ICRA)*. IEEE, 2008, pp. 1150–1155.
- [12] H. Kimura, F. Kajimura, D. Maruyama, M. Koseki, and N. Inou, “Flexible hermetically-sealed mobile robot for narrow spaces using hydrostatic skeleton driving mechanism,” in *2006 IEEE/RSJ International Conference on Intelligent Robots and Systems*. IEEE, 2006, pp. 4006–4011.
- [13] M. E. Ingram, “Whole skin locomotion inspired by amoeboid motility mechanisms: Mechanics of the concentric solid tube model,” Ph.D. dissertation, Virginia Polytechnic Institute and State University, 2006.
- [14] D. J. Anhalt, J. B. Herron *et al.*, “Toroidal propulsion and steering system,” 2006, uS Patent 7,044,245.

- [15] J. Gao, X. Gao, W. Zhu, J. Zhu, and B. Wei, "Design and research of a new structure rescue snake robot with all body drive system," in *2008 IEEE International Conference on Mechatronics and Automation (ICMA)*. IEEE, 2008, pp. 119–124.
- [16] H. Dugoff and I. Robert Ehlich, "Model tests of bouyant screw rotor configurations," *Journal of Terramechanics*, vol. 4, no. 3, pp. 9–22, 1967.
- [17] M. Neumeyer and B. Jones, "The marsh screw amphibian," *Journal of Terramechanics*, vol. 2, no. 4, pp. 83–88, 1965.
- [18] R. G. Schrader, "Amphibious mud and xwater v veehcle," 1966, uS Patent 3,229,658.
- [19] S. J. Knight, E. S. Rush, and B. G. Stinson, "Trafficability tests with the marsh screw amphibian," *Journal of Terramechanics*, vol. 2, no. 4, pp. 31–50, 1965.
- [20] H. Liang, Y. Guan, Z. Xiao, C. Hu, and Z. Liu, "A screw propelling capsule robot," in *2011 IEEE International Conference on Information and Automation (ICIA)*. IEEE, 2011, pp. 786–791.
- [21] D. Koh, J. Yang, and S. Kim, "Centipede robot for uneven terrain exploration: Design and experiment of the flexible biomimetic robot mechanism," in *2010 3rd IEEE RAS and EMBS International Conference on Biomedical Robotics and Biomechatronics (BioRob)*. IEEE, 2010, pp. 877–881.
- [22] R. Primerano, D. Wilkie, and W. Regli, "Toward a multi-disciplinary model for bio-robotic systems," in *2008 IEEE International Conference on Robotics and Automation (ICRA)*. IEEE, 2008, pp. 257–263.
- [23] R. D. Allen, "Multi-legged, walking toy robot," 1995, uS Patent 5,423,708.
- [24] H. G. Grimm, "Animated toy," 1958, uS Patent 2,827,735.

- [25] M. T. McKittrick Jr and N. DeAnda, “Animated toy,” 1986, uS Patent 4,629,440.
- [26] L. L. Kramer, “Motor operated ambulatory vehicle,” 1967, uS Patent 3,331,463.
- [27] H. Tsukagoshi, A. Kitagawa, M. Ito, K. Ooe, I. Kiryu, and T. Kochiya, “Bari-bari-ii: Jack-up rescue robot with debris opening function,” in *2008 IEEE International Conference on Robotics and Automation (ICRA)*, 2008, pp. 2209–2210.
- [28] K. Takahashi, Y. Goto, and T. Nakamura, “Development of the wall climbing robot using a spiral style wave transmission system move mechanism,” in *2012 JSME Conference on Robotics and Mechatronics*. JSME, 2012, pp. 2A1–O02.
- [29] S. Hirose, H. Ohno, T. Mitsui, and K. Suyama, “Design of in-pipe inspection vehicles for $\varphi 25$, $\varphi 50$, $\varphi 150$ pipes,” in *1999 IEEE International Conference on Robotics and Automation*, vol. 3. IEEE, 1999, pp. 2309–2314.
- [30] G. Gabrielli and T. Von, *What price speed?: specific power required for propulsion of vehicles*, 1950.
- [31] P. Gregorio, M. Ahmadi, and M. Buehler, “Design, control, and energetics of an electrically actuated legged robot,” *IEEE Transactions on Systems, Man, and Cybernetics, Part B: Cybernetics*, vol. 27, no. 4, pp. 626–634, 1997.
- [32] G. Endo and S. Hirose, “Study on roller-walker improvement of locomotive efficiency of quadruped robots by passive wheels,” *Advanced Robotics*, vol. 26, no. 8-9, pp. 969–988, 2012.
- [33] ———, “Study on roller-walker - energy efficiency of roller-walk -,” in *2011 IEEE International Conference on Robotics and Automation (ICRA)*, 2011, pp. 5050–5055.

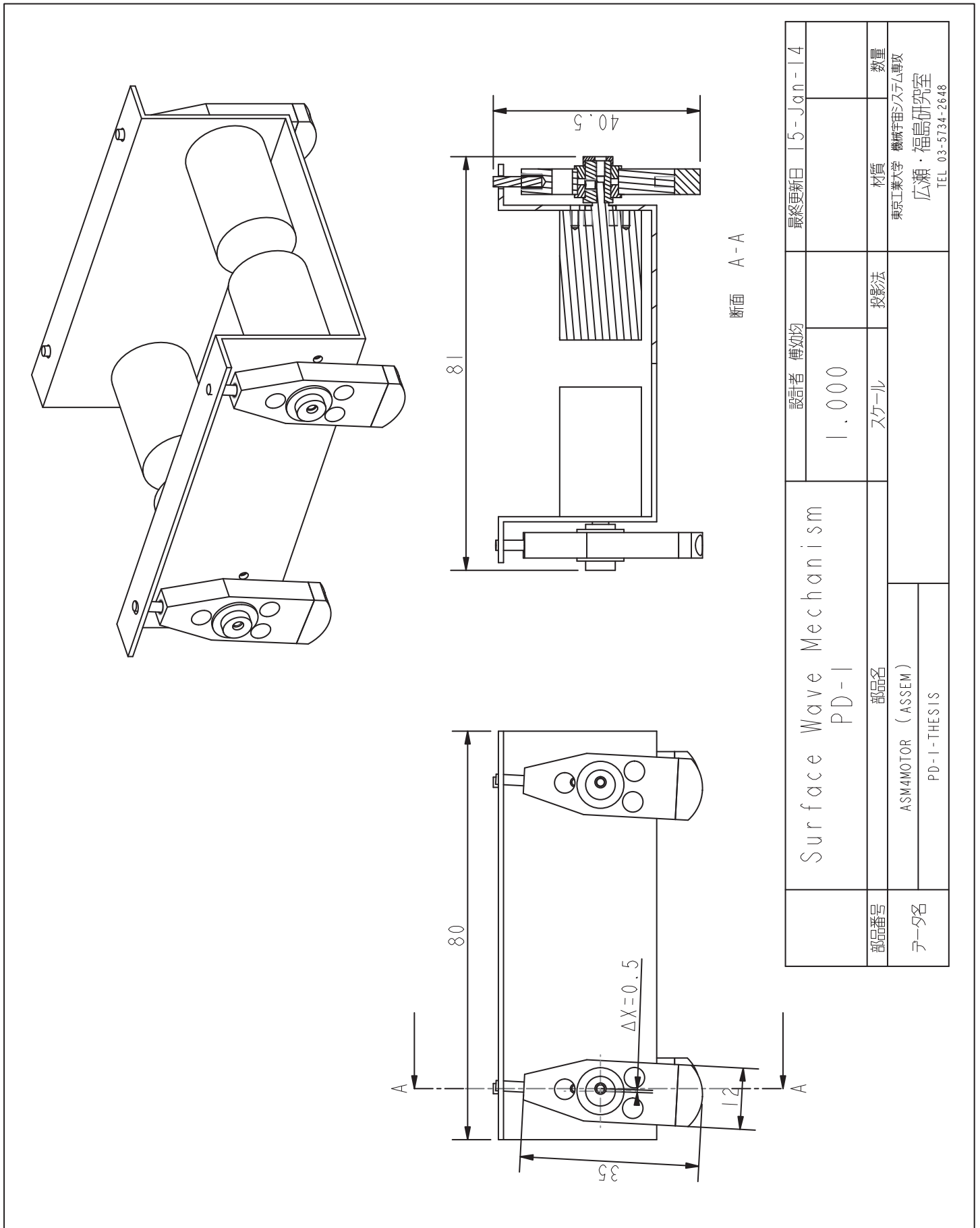
- [34] E. Moore and M. Buehler, “Stable stair climbing in a simple hexapod robot,” DTIC Document, Tech. Rep., 2001.
- [35] M. Ahmadi and M. Buehler, “The arl monopod ii running robot: control and energetics,” in *1999 IEEE International Conference on Robotics and Automation*, vol. 3, 1999, pp. 1689–1694 vol.3.
- [36] W. Provancher, S. Jensen-Segal, and M. Fehlbeg, “Rocr: An energy-efficient dynamic wall-climbing robot,” *IEEE/ASME Transactions on Mechatronics*, vol. 16, no. 5, pp. 897–906, 2011.
- [37] E. F. FUKUSHIMA, H. NAKAMOTO, R. DAMOTO, and S. HIROSE, “Development of off-road vehicle” helios-vi”. optimal load sensitive control for continuously variable transmissions.” *Nippon Robotto Gakkai Gakujutsu Koenkai Yokoshu*, vol. 19, pp. 953–954, 2001.
- [38] T. Sato and S. Hirose, “The development of automatic dual mode transmission using hysteresis magnetic coupling,” *Proceedings of the 1995 JSME Conference on Robotics and Mechatronics*, vol. 1995, 1995.
- [39] Y. Teranishi and S. Hirose, “Development of a load-sensitive dual states transmission with a twoway clutch,” *Proceedings of the 2007 JSME Conference on Robotics and Mechatronics*, vol. 2007, 2007.
- [40] T. Hagiwara and S. Hirose, “Development of load-sensitive continuously variable rotary transmission vol.1 a proposition of basic mechanism,,” *Proceedings of the 2001 JSME Conference on Robotics and Mechatronics*, vol. 2001, p. 16, 2001.
- [41] S. Hirose, C. Tibbetts, and T. Hagiwara, “Development of x-screw: a load-sensitive actuator incorporating a variable transmission,” in *1999 IEEE Inter-*

national Conference on Robotics and Automation, vol. 1, 1999, pp. 193–199
vol.1.

Appendix A

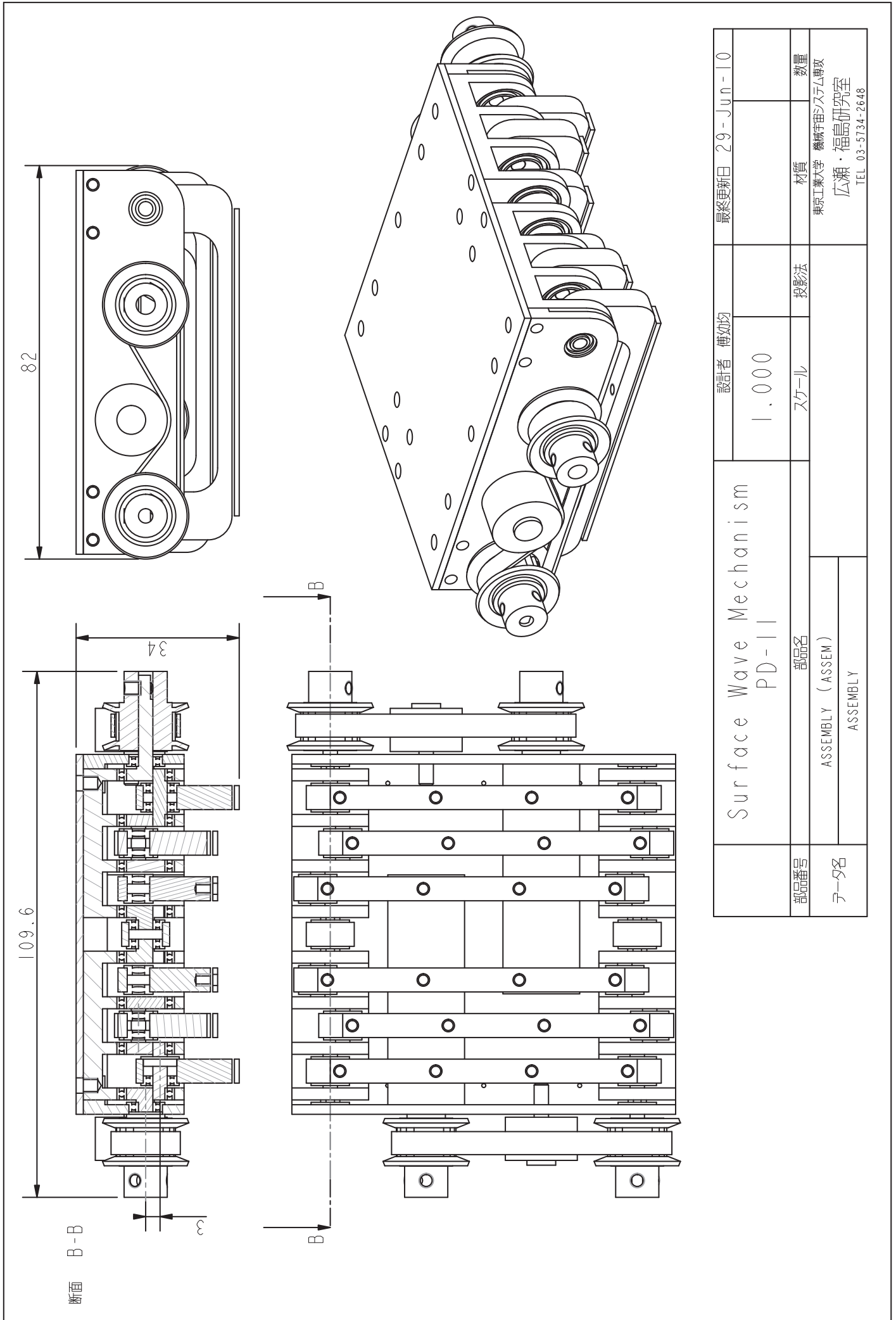
CAD Drawings

In this study, Pro ENGINEER Wildfire 4.0 was used for making CAD drawings. The assembly drawings of the prototypes are shown in the following pages.



Surface Wave Mechanism PD-I		設計者 備如均	最終更新日 5-Jan-14
部品番号	部品名	スケール	投影法
ASM4MOTOR (ASSEM)		1.000	
メーカー名	PD-I-THESIS	材質	数量
		東京工業大学 機械宇宙システム専攻	
		広瀬・福島研究室	
		TEL 03-5734-2648	

Fig. A.0.1: Drawing of Surface Wave Mechanism PD-I



Surface Wave Mechanism PD-II		設計者 傅如均	最終更新日 29-Jun-10
1.000	スケール	投影法	数量
部品番号	部品名	材質	数量
テータ名	ASSEMBLY (ASSEM)	東京工業大学 機械宇宙システム専攻	
	ASSEMBLY	広瀬・福島研究室	
		TEL 03-5734-2648	

Fig. A.0.2: Drawing of Surface Wave Mechanism PD-II

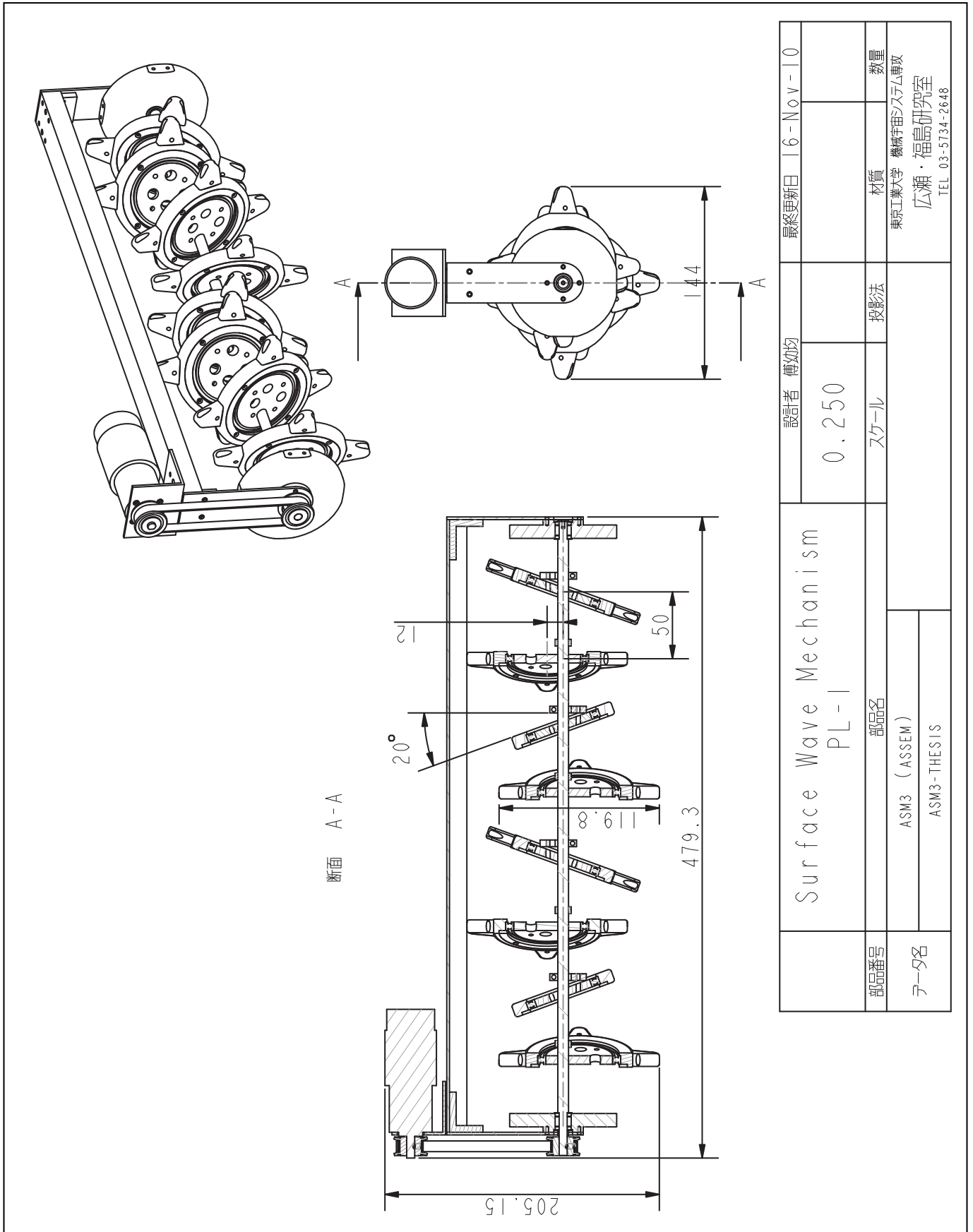


Fig. A.0.3: Drawing of Surface Wave Mechanism PL-I

Appendix B

Trajectory Simulation

```

//circle.m//
th=linspace(0,2*pi,1000);
r=1;
x=r*cos(th);
y=r*sin(th);
c=[x;y;linspace(0,0,1000);ones(1,1000)]; //circle
angx=pi/180*0;
Tx=[1,0,0,0;0,cos(angx),-sin(angx),0;0,sin(angx),cos(angx),0;0,0,0,1]; //x-rotation
angy=pi/180*10;
Ty=[cos(angy),0,sin(angy),0;0,1,0,0;-sin(angy),0,cos(angy),0;0,0,0,1]; //y-rotation

c1=Ty*Tx*c; //transformed circle
c1(2,:)=c1(2,:)+0.05; //y-eccentricity

angz=pi/2;
Tz=[cos(angz),-sin(angz),0,0;sin(angz),cos(angz),0,0;0,0,1,0;0,0,0,1];
c1=Tz*c1;

```

```
figure(1);
hold on;
grid on;
view([0,90]);
axis([-1.5 1.5 -1.5 1.5 -1.5 1.5]);
zaxis=[0,0;0,0;-2,2];
plot3(zaxis(3,:),zaxis(2,:),zaxis(1,:), 'r', 'LineWidth', 2);    //show z-axis
xlabel('Z'); ylabel('Y'); zlabel('X');
plot3(c1(3,:),c1(2,:),c1(1,:), 'm', 'LineWidth', 3);

n=1;
trail=0; m=0; p=0;           //initialize
angz=pi/12;

for ang=0:angz:pi*2;
    Tz=[cos(angz),-sin(angz),0,0;sin(angz),cos(angz),0,0;0,0,1,0;0,0,0,1];
    c1=Tz*c1; //rotate along z-axis

    [m,p]=min(c1,[],2);
    trail(1,n)=c1(1,p(2));
    trail(2,n)=c1(2,p(2));
    trail(3,n)=c1(3,p(2));

    // plot3(zaxis(3,:),zaxis(2,:),zaxis(1,:), 'r', 'LineWidth', 2);    //show z-axis

    plot3(c1(3,:),c1(2,:),c1(1,:), 'c');

    if n < 13
        plot3(trail(3,1:n),trail(2,1:n),trail(1,1:n), 'k', 'LineWidth', 2);
```

```
else
    plot3(trail(3,1:n),trail(2,1:n),trail(1,1:n),'r','LineWidth',2);
end

// pause(0.2);
n=n+1;
end

// plot3(c1(3,:),c1(2,:),c1(1,:), 'c');

figure(2);
hold on;
grid on;

subplot(2,2,1);
plot(trail(3,1:13),trail(1,1:13),'k',trail(3,13:25),trail(1,13:25),'r','LineWidth',2); //zx-plane
title('z-x plane'); axis equal; axis([-0.3 0.3 -0.3 0.3]);
xlabel('Z'); ylabel('X');

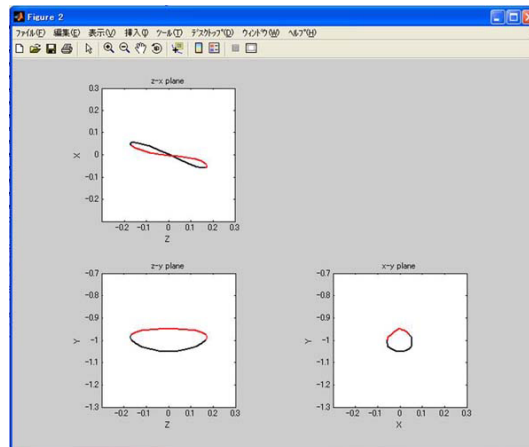
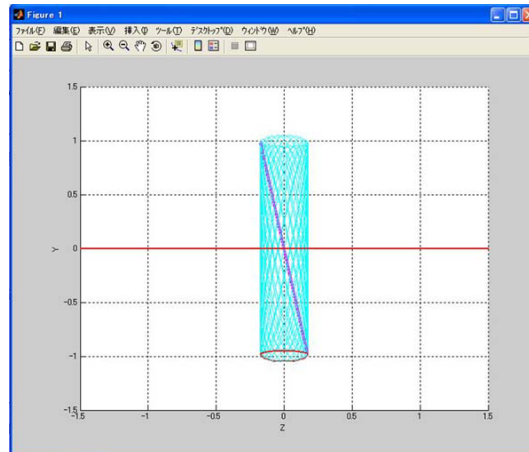
subplot(2,2,4);
plot(trail(1,1:13),trail(2,1:13),'k',trail(1,13:25),trail(2,13:25),'r','LineWidth',2); //yx-plane
title('x-y plane'); axis equal; axis([-0.3 0.3 -1.3 -0.7]);
xlabel('X'); ylabel('Y');

subplot(2,2,3);
plot(trail(3,1:13),trail(2,1:13),'k',trail(3,13:25),trail(2,13:25),'r','LineWidth',2); //yz-plane
title('z-y plane'); axis equal; axis([-0.3 0.3 -1.3 -0.7]);
xlabel('Z'); ylabel('Y');
```


Appendix B. Trajectory Simulation

//END of circle.m//

Results of execution:



Appendix C

Calculation of Contact Angle α

```
//alpha-calculation.m//  
e=[8;2;0];    //eccentric distance  
r=46.55;     //radius (mm)  
P0=[0;-r;0];  
  
for j=1:1:360,  
    xi=xi-data(j)/180*pi;    //xi-data is the data of rotational angle recorded in exper-  
    iment  
    phi=phi-data(j)/180*pi;    //phi-data is the data of inclination angle recorded in  
    experiment  
  
    for i=1:1:360,  
        th=i/180*pi;  
        P(:,i)=R('z',xi)*R('y',phi)*(e+R('z',th)*P0);  
    end  
  
// Find contact point: differential of Py
```

```
// dPy/d(th)=sin(xi)*cos(phi)*cos(th)*r+cos(xi)*sin(th)*r=0
// th=atan(-tan(xi)cos(phi))

thCP(j)=atan(-tan(xi)*cos(phi));
CP(:,j)=R('z',xi)*R('y',phi)*(e+R('z',thCP(j))*P0);    // contact point

if CP(2,j)>0
    thCP(j)=thCP(j)+pi;
    CP(:,j)=R('z',xi)*R('y',phi)*(e+R('z',thCP(j))*P0);    // contact point
end

if thCP(j)>0
    thCP(j)=thCP(j)+2*pi;
end

// find vecT , alpha
//    vecT: tangential direction of the disc at contact point
//    alpha: included angle of vecT and xy-plane

t(:,j) = vecT(r,e(1),e(2),phi,xi,thCP(j));
vectorT=[CP(:,j),CP(:,j)+t(:,j)];
alpha(j) = atan2(t(3,j),t(1,j))/pi*180;    // angle  $\alpha$ 

end

//END of alpha-calculation.m//
```